



Review of low-GWP refrigerant pool boiling heat transfer on enhanced surfaces



Lingnan Lin*, Mark A. Kedzierski

National Institute of Standards and Technology, Gaithersburg, MD 20899, USA

ARTICLE INFO

Article history:

Received 25 July 2018

Received in revised form 27 November 2018

Accepted 27 November 2018

Keywords:

Low-GWP refrigerants

Pool boiling

Heat transfer

Enhanced surfaces

ABSTRACT

Global warming mitigation efforts have stimulated investigations of a new generation of low-GWP refrigerants. Because some of the proposed low-GWP refrigerants have unfavorable characteristics (e.g., flammability and toxicity), a small refrigerant charge is desirable. Compact heat exchangers with enhanced surfaces facilitate small refrigerant charge by having a large heat exchanger surface area to heat exchanger volume ratio. This paper reviews the current state-of-the-art for pool boiling heat transfer of low-GWP refrigerants on enhanced surfaces. An overview for the enhanced surface manufacturing technique is given along with detailed reviews of the heat transfer measurements and predictions for many of the low-GWP refrigerants, including the hydrofluoroolefin (HFO) class, the hydrocarbon (HC) class, carbon dioxide (CO₂), and ammonia (NH₃). The overview of the predictive methods includes mechanistic models and correlations for pool boiling on enhanced surfaces. Based on the surveyed literature, existing shortfalls are identified and suggestions for future studies are proposed.

Published by Elsevier Ltd.

Contents

| | |
|---|------|
| 1. Introduction ¹ | 1280 |
| 2. Enhanced surfaces | 1281 |
| 2.1. Structured surfaces | 1282 |
| 2.2. Porous surfaces | 1283 |
| 2.3. Other surfaces | 1284 |
| 3. Measurements for low-GWP refrigerants on enhanced surfaces | 1285 |
| 3.1. Hydrofluoroolefins | 1288 |
| 3.2. Hydrocarbon | 1290 |
| 3.3. Ammonia and carbon dioxide | 1293 |
| 4. Predictive methods | 1294 |
| 4.1. Structured surfaces | 1294 |
| 4.2. Porous surfaces | 1300 |
| 5. Conclusions and suggestions | 1301 |
| Conflict of interest | 1301 |
| Acknowledgement | 1301 |
| References | 1301 |

* Corresponding author.

E-mail address: lingnan.lin@nist.gov (L. Lin).

Nomenclature

| | |
|------------|---|
| A | area [m ²] |
| A_H | Hamaker constant |
| Ar | Archimedes number |
| a | constants |
| Bo | Bond number |
| b | constants |
| C_p | specific heat capacity |
| C, c | constants |
| D | diffusion coefficient |
| D_h | hydraulic diameter [m] |
| d | diameter [m] |
| F | force |
| F_E | HTC enhancement factor (ratio of enhanced surface HTC to plain surface HTC) |
| Fr | Froude number |
| f | frequency |
| G_{t-s} | geometric factor |
| H | height [m] |
| h | heat transfer coefficient [W/(m ² K)] |
| i_{lv} | latent heat of vaporization (J/kg) |
| Ja^* | modified Jacob number |
| k | thermal conductivity [W/(m K)] |
| L | length [m] |
| La | Laplace constant |
| N | number |
| N_{Sn} | Scriven number |
| N_{conf} | confinement number |
| n_s | nucleation site density [m ⁻²] |
| P | pressure [Pa] |
| P^* | reduced pressure |
| p | pitch [m] |
| Q | heat energy [W] |
| q | heat flux [W/m ²] |
| R, r | radius [m] |
| R_x | geometry enhancement factor |
| S | nucleate boiling correction factor |
| s | spacing [m] |
| T | temperature [K] or [°C] |
| t | time [s] |
| V | volume [m ³] |
| W | width [m] |
| We | Weber number |
| u | velocity [m/s] |
| X_{tt} | Martinelli parameter |
| x | vapor quality |

Greek symbols

| | |
|----------|---|
| α | thermal diffusivity [m ² s ⁻¹] |
| β | helix angle [°]; coefficients |

| | |
|---------------|--------------------------------------|
| δ | thickness [m] |
| ε | void fraction |
| σ | surface tension |
| Φ | two-phase multiplier |
| η | surface enlargement ratio |
| θ | bubble's phase period; contact angle |
| μ | dynamic viscosity [Pa/s] |

Subscripts

| | |
|-----|--------------------------|
| ap | active pores |
| bb | bubble |
| cb | convective boiling |
| cap | capillary |
| ch | channel |
| ex | external |
| g | growth |
| H | horizontal |
| l | liquid |
| la | latent |
| lo | liquid only |
| lv | least volatile component |
| m | mean; meniscus |
| mv | most volatile component |
| nb | nucleate boiling |
| ne | non-evaporating |
| V | vertical |
| v | vapor |
| p | particles |
| pb | pool boiling |
| s | saturation |
| tp | two-phase |
| tun | tunnel |
| w | waiting |

Abbreviation

| | |
|--------|---|
| HVAC&R | heating, ventilating, air-conditioning, and refrigerating |
| HFC | hydrofluorocarbons |
| HTC(s) | heat transfer coefficient(s) |
| GWP | global warming potential |
| EU | European Union |
| HFO | hydrofluoroolefin |
| HC | hydrocarbon |
| EHD | electrohydrodynamic |
| EDM | electric discharge machining |
| SLM | selective laser melting |
| CVD | chemical vapor deposition |

1. Introduction¹

In recent decades, concern over greenhouse gases associated with global warming has grown to include refrigerant emissions. Many of the hydrofluorocarbons (HFCs) that are currently used in heating, ventilation, air-conditioning and refrigeration (HVAC&R) systems since the early 1990s have a relatively large global warm-

ing potential (GWP) (>1000). To mitigate the global warming effect, many countries are taking actions to reduce the use of HFC refrigerants. In 2014, the European Union (EU) issued the F-gas Regulation (applied from January 2015) to mandate the phase-down of HFCs [1]. On October 15th, 2016, the 197 Parties to the Montreal Protocol adopted the Kigali Amendment for HFC phase-down, and committed to cutting the production and consumption of HFCs by more than 80% over the next 30 years [2]. The growing international emphasis on HFC phase-down has stimulated the interest of industry and academia in alternative refrigerants with low GWP.

The current low-GWP refrigerants proposed as HFC replacements mainly include the hydrofluoroolefin (HFO) class, the

¹ Certain trade names and company products are mentioned in the text or identified in an illustration in order to adequately specify the experimental procedure or equipment. In no case does such an identification imply recommendation or endorsement by the National Institute of Standards and Technology, USA, nor does it imply that the products are necessarily the best available for the purpose.

hydrocarbon (HC) class, carbon dioxide (CO₂), and ammonia (NH₃). Though these refrigerants have very low GWP values (less than 20), each of them has unfavorable characteristics that make them unsuitable as a direct drop-in alternative (Table 1), with flammability and toxicity being the most common concerns. As a result, many refrigeration systems using low-GWP refrigerants are required to have a low-refrigerant-charge. For example, the current charge limits for hydrocarbon refrigerants are as low as 150 g in the United States and Europe [3], though international efforts to raise the hydrocarbon charge limit are still ongoing. It is also strongly recommended to use HFOs and ammonia with a low charge based on safety and economic considerations [4–6]. It is expected that low refrigerant charge systems will become more prevalent in the near future. The refrigerant charge can be reduced by several methods, such as the use of enhanced heat transfer equipment, optimization of the heat exchanger design, and the use of more efficient heat exchanger techniques (e.g., falling film). Heat transfer enhancements can be used to reduce the size of the heat exchangers and to increase the system cycle performance; hence, these enhancements are of great importance for low-GWP refrigerant applications.

Pool boiling is the primary mode of heat transfer that occurs in flooded evaporators that are used for refrigeration and air-conditioning applications. The techniques for pool boiling heat transfer enhancement can be categorized in two general types: passive and active techniques [7]. Passive techniques involve special surface geometries, fluid additives, or insert devices for enhancement. The common passive techniques include enhanced surface [8–10], nanofluids [11,12], displaced inserts [13–15], and swirl flow device [15,16]. Active techniques require external power input, such as ultrasound [17], mechanical vibration [18,19], electrohydrodynamic (EHD) [20,21], and magnetic field [22]. Currently, commercially-available heat-transfer enhancement devices mainly employ passive techniques, because active techniques generally result in higher cost and may cause noise, safety, or reliability problems.

The enhanced surface is the most extensively used technique for pool boiling heat transfer augmentation in the refrigeration and air-conditioning industry. For example, nearly all water chillers using shell-and-tube heat exchangers employ enhanced tubes. Enhanced surfaces can be applied to increase efficiency and/or reduce the heat exchanger size and, in turn, reduce the low-GWP refrigerant charge. Therefore, the measurements and predictive methods for pool boiling heat transfer are necessary for the design of flooded evaporators using low-GWP refrigerants. They are also of importance in studying the certain domains of flow boiling with heat transfer being governed by the processes connected to bubble formation and detachment at active nucleation sites [23].

This paper provides a comprehensive review of pool boiling heat transfer for low-GWP refrigerants on enhanced surfaces. The enhanced surface technology is reviewed (Section 2), followed by detailed reviews on the state-of-the-art of measurements for boiling heat transfer with low-GWP refrigerants on enhanced surfaces (Section 3). The review is limited to HFO class, HC class, NH₃, and CO₂ refrigerants. The paper concludes with a review of the existing predictive methods for pool boiling on enhanced surfaces (Section 4) and suggests future work.

2. Enhanced surfaces

The enhanced boiling surfaces typically have special geometries that provide higher heat transfer coefficients in terms of projected area compared with plain (or smooth) surfaces. The fact that “roughness” enhances nucleate boiling heat transfer has been known since 1931 when Jakob observed that the boiling heat transfer coefficients (HTC) for water on a grooved surface were about three times higher than those of a plain surface [24]. As reported by Jakob, however, such enhancement only lasted for a short time, which was described as the “aging effect.” Due to the “aging effect”, rough surfaces were considered as an unpractical concept for the next two decades. In the period of 1955–1965, numerous fundamental studies were made toward understanding the boiling mechanism [25–30]. Researchers started to realize the importance of nucleation sites and made attempts to create effective artificial nucleation sites. In 1968, Milton patented one of the first practical enhanced surface geometries which was formed by coating a sintered layer of copper particles (commercially known as “High-Flux”) [31]. After that, many enhanced surface geometries were invented and continue to be revised, improved, and developed today. Industrial research plays a key role in the development of commercial surface enhancements, where most of the geometries are reported in patents. A detailed evolution of enhanced boiling surfaces is provided by Webb’s review papers [8,32].

For pool boiling enhancement of refrigerants, the enhanced surface generally features reentrant cavities with connecting tunnels and mouth openings smaller than the cavity. Reentrant cavities can trap more vapor compared with conical and cylindrical cavities that exist on smooth surfaces, especially for highly wetting fluids like refrigerants (Fig. 1) [33]. More trapped vapor enables reentrant cavities to generate larger embryonic bubbles which require less superheat to nucleate at a specified heat flux. Hence, surfaces having reentrant cavities yield much higher nucleation site densities than plain surfaces and thereby, greater heat transfer performance. Reentrant cavities can be formed through mechanical metal

Table 1
Characteristics of low-GWP refrigerants [4,128,129].

| Type | Typical refrigerants | GWP ₁₀₀ [*] | Advantages | Disadvantages |
|-----------------------------------|----------------------|---------------------------------|---|--|
| Hydrofluoroolefin (HFO) | R1234yf | <1 | – Non-toxic – Similar thermo-physical properties to the existing HCFCs | – High cost – Slightly flammable |
| | R1234ze(E) | <1 | | |
| | R1234ze(Z) | <1 | | |
| | R1233zd(E) | <1 | | |
| Hydrocarbon (HC) | R290 | 3 | – Efficient – Low cost | – Highly flammable |
| | R600 | 4 | | |
| | R600a | 3 | | |
| | R1270 | 2 | | |
| Carbon dioxide (CO ₂) | R744 | 1 | – Non-flammable – Non-toxic | – Not enough efficient – High pressure (lead to high cost for components) |
| Ammonia (NH ₃) | R717 | 0 | – Very efficient – Low cost | – Toxic – Slightly flammable |

^{*} Literature value from the IPCC Assessment Reports [128,129].

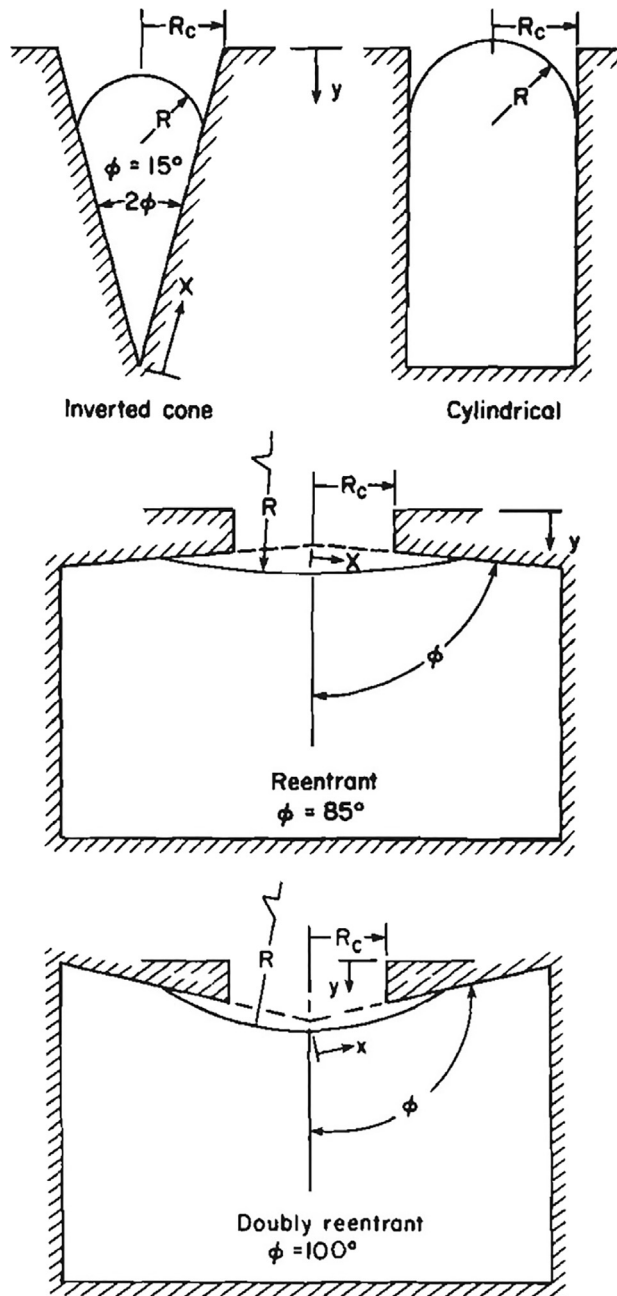


Fig. 1. Vapor-liquid interface in cavities of different shapes. (from Webb [33]).

forming processes and porous coatings, which are two basic fabrication types of enhanced surfaces for pool boiling.

2.1. Structured surfaces

Structured surfaces are formed by lifting the base surface of a plain tube to form integral-fins and have been commercially available since the 1930s [34]. Further cold metal working (or mechanical machining) of the integral fin produces more advanced and higher performing enhancements. One may employ one or several cold-working methods (e.g., rolling, notching) using a specially designed apparatus to form the enhanced structure that generally consists of pores and/or interconnected tunnels below the surface. The resulting boiling enhancement is due to both the increase in the surface area and the improved bubble nucleation behavior. Four of the classical structured surfaces are:

- *Integral-fin surface.* Fig. 2a shows a standard integral-fin tube (also called low fin), which is the most basic form of enhanced tubes. Most of the structured surfaces are fabricated by lifting the fins from the wall of a plain tube via a rolling process. Generally, the integral-fin boiling tubes have 748–1970 fins per meter (i.e., 19–50 fins per inch) with fin height from 0.8 mm to 1.5 mm [35]. Although the integral-fin does not have manufactured reentrant cavities, the integral fin can increase the nucleation site density as compared to a plain tube by encouraging bubble agglomeration between the fins and bubble nucleation on the fin-sides [36].
- *GEWA series.* Fig. 2b illustrates a T-shaped finned tube made by flattening the fins on the integral-fin tube, which has been commercialized as GEWA-T, -TW, and -TX. Fig. 2c is a Y-finned tube made by notching the fins on the integral-fin tube, which has been commercialized as GEWA-SE and -YX. The T- or the Y-shaped fins create reentrant tunnels, which causes heat transfer enhancement beyond the surface area enlargement. These two geometries, patented by Saier et al. in 1979 [37], are the earliest GEWA enhanced surfaces. Based on these geometries, several variants of the GEWA enhanced boiling surface were developed by Wieland-Werke over the next 30 years. For example, GEWA-PB is an enhanced boiling surface specially designed for hydrocarbons, and it is widely used in propane chillers. The latest version, GEWA-B series, is designed for boiling enhancement for different purposes (e.g., GEWA-B6 for highest performance, GEWA-BHV for high viscosity media, GEWA-BLF for high fouling tendency [38]).
- *Thermoexcel-E.* Fig. 2d shows a Thermoexcel-E tube made from a low fin tube with “sawtooth” fins, i.e., having a small portion cut from the fin tips. The sawtooth-shaped fins are bent horizontally to form reentrant tunnels with spaced pores on top of the tunnels created by the cut-outs. The geometry of Thermoexcel-E was patented by Fujie et al. [39].
- *Turbo-B series.* The original Turbo-B outer surface (Fig. 2e) was introduced by Cunningham and Campbell in 1985 [40]. The Turbo-B has a grid pattern consisting of rectangular flattened blocks separated by narrow gaps which overlie a relatively wider sub-surface tunnel. The geometry is formed by successive cross-grooving and rolling operations on an integral-fin surface. Fig. 2f and g depict the outer surface geometries of Turbo-BII and Turbo-BIII, respectively, which were patented by Thors et al. [41]. The structures on Turbo-BII and Turbo-BIII are made by deforming helical fins on an integral-in tube and notching to provide pores for nucleation. Nowadays, there are several variants evolved from Turbo-B, such as Turbo-B5, -ESP, -EHPII, and -EPT. It’s noted that the Turbo-B type tube also has internal helical grooves for in-tube single-phase heat transfer enhancement.

Besides the classical geometries illustrated above, there are numerous commercially available geometries developed over recent decades. Table 2 lists the U.S. patents for structured boiling surfaces issued after 2005. In total, eleven patents are found in this survey. Earlier studies on structured surfaces were comprehensively reviewed by Webb [7] and Thome [42].

In recent years, several novel techniques have been developed for more precise fabrication, such as electric discharge machining (EDM). In addition, structures in microscale or even nanoscale can be produced by selective laser melting (SLM), femtosecond laser process, and photolithography and etching. Fig. 3 shows selected surface structures fabricated by these techniques. The existing studies on these novel techniques are mostly limited to the flat surfaces that are mainly used for electronic cooling application. However, a few studies are found for tubular surfaces that are used for refrigerant applications. Details on the enhanced

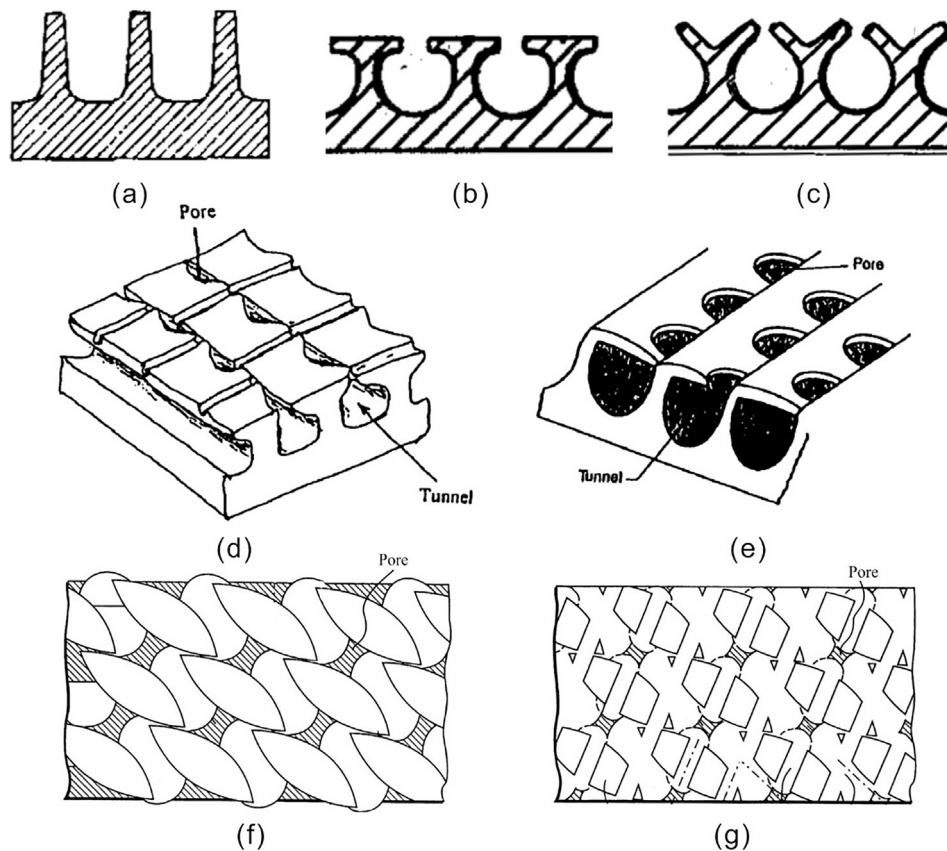


Fig. 2. Illustration of seven classical structured surfaces. (a) Integral-fin surface; (b) T-shaped finned surface, from Saier et al. [37]; (c) Y-shaped finned surface, from Saier et al. [37]; (d) Thermoexcel-E tube surface, from Chien [76]; (e) Turbo-B tube surface, from Chien [76]; (f) Turbo-BII tube surface, from Thors et al. [41]; (g) Turbo-BIII tube surface, from Thors et al. [41].

Table 2

U.S. patents on structured boiling surface issued after 2005.

| Patent no. | Issued date | Inventers | Title |
|-------------|-------------|-----------------|---|
| US9618279B2 | 2017/4/11 | Lutz et al. | Evaporator tube having an optimized external structure |
| US9038710B2 | 2015/5/26 | Cao et al. | Finned tube for evaporation and condensation |
| US8899308B2 | 2014/12/2 | Beutler et al. | Heat exchanger tube and method for producing it |
| US8857505B2 | 2014/10/14 | Beutler et al. | Structured heat exchanger tube and method for the production thereof |
| US8281850B2 | 2012/10/9 | Beutler et al. | Evaporator tube with optimized undercuts on the groove base |
| US8162039B2 | 2012/4/24 | Cao et al. | Finned tube for condensation and evaporation |
| US7841391B2 | 2010/11/30 | Hao et al. | Flooded type evaporating heat-exchange copper tube for an electrical refrigeration unit |
| US7789127B2 | 2010/9/7 | Lu et al. | Heat transfer tubes for evaporators |
| US7254964B2 | 2007/8/14 | Thors and Tyler | Heat transfer tubes, including methods of fabrication and use thereof |
| US7178361B2 | 2007/2/20 | Thors and Tyler | Heat transfer tubes, including methods of fabrication and use thereof |
| US6913073B2 | 2005/7/5 | Beutler et al. | Heat transfer tube and a method of fabrication thereof |

boiling surfaces fabricated by these novel techniques can be found in the reviews by Shojaeian and Koşar [9], Leong et al. [10], and Kim et al. [43].

2.2. Porous surfaces

As indicated by its name, a porous surface has an interconnected porous matrix which can also increase surface area and active nucleation site density. The porous matrix can be made of either the same material as the base surface or a different one. The solid network of the matrix could be composed of particles (most common), tubes, wires, meshes, foam cells, and so on. The matrix thickness and pore size are the two most important parameters of a porous surface, and their optimal values mainly depend on the fluid properties. The following are common techniques for fabricating a porous surface.

– *Sintering.* The fabrication of a typical sintered surface can be summarized in three steps: powder preparation, compaction, and fusion. Generally, powders are first mixed with “lubricant”, which helps compaction and acts to inhibit powder agglomeration. The liquid powder slurry is subsequently covered on the surface. The next step is to heat the slurry-coated surface to melt the powder and eventually vaporize the “lubricant”, during which the powders and the surface come in contact to form “necks” that create loose bonds. Then the temperature is elevated to grow the “neck” and eventually fuse the particles and surface together. High-Flux is an enhanced boiling tube made by powder-sintering (Fig. 4a [44]), which has been commercialized since around 1970 when Milton’s patents were issued [31,45,46]. Besides powders, other forms, such as metal mesh (Fig. 4b [47]) and metal foam (Fig. 4c [48]) can be sintered on surfaces to produce boiling enhancements.

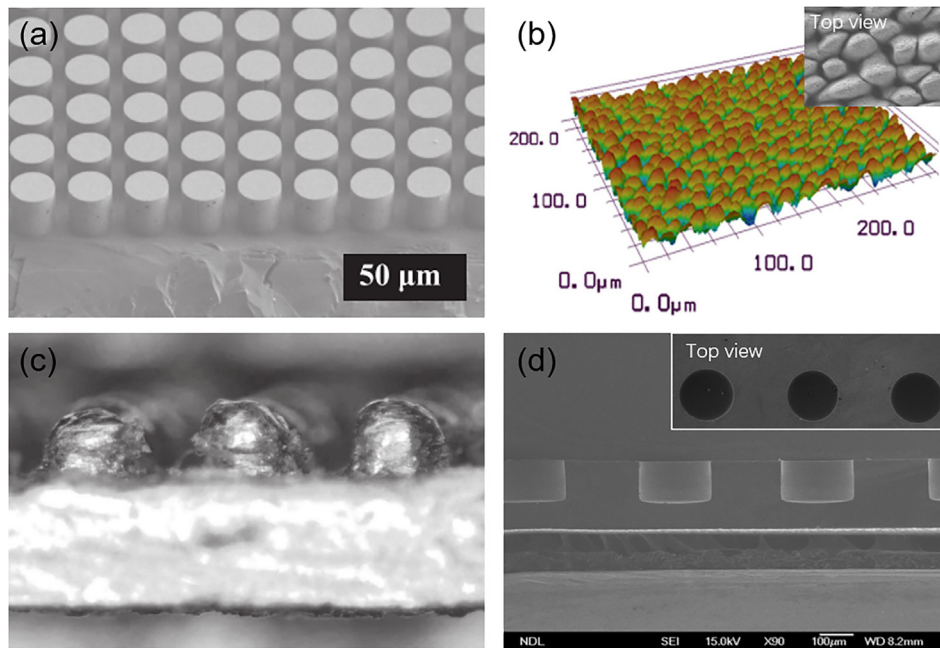


Fig. 3. Selected structured surfaces fabricated by novel techniques. (a) Silicon chip with Circular micro-pillar arrays made by deep reactive ion etching, from Kim et al. [125]; (b) Stainless steel surface with mound-like microstructures made by femtosecond laser process, from Kruse et al. [126]; (c) Structured surface made by selective laser melting (SLM), from Ho et al. [114]; (d) Silicon surface with micro cylinder pores made by dry etching process, from Yu et al. [127].

- *Spray coating.* This process is one in which fine metallic or non-metallic particles are sprayed on a surface to form a coating. In this process, an energy source is used to melt the feedstock material and accelerate the particles toward the surface. Spray coating processes are generally classified by the energy source that is used to create the surface. Combustion flame (flame spraying, detonation spraying, high velocity spraying), electric discharge (plasma spraying, arc spraying), beams (laser spraying), kinetic energy (cold kinetic spraying), or molten liquid (liquid spraying) are some examples. Powder, wire, or rods are used as the feedstock for the coating [49]. Fig. 4d and e show a 95.4 μm-thick Cu coating made by flame spraying and a 300 μm-thick Mo coating made by plasma spraying, respectively [50,51].
- *Electrochemical deposition (or electroplating).* Compared with sintering and spray coating, electrochemical deposition is a simpler and a less expensive method for generating micro/nanoporous structures. By applying direct current on a solution containing the ion or chemical complex of the desired metal, the metal deposits onto the cathode surface and forms a coating. The temperature, current density, and pH are key operating parameters for controlling the coating structures [52]. Fig. 4f and g show a copper nanowire coating and a structurally strengthened copper micro-porous coating, respectively, both made by electrochemical deposition [53,54].
- *Chemical vapor deposition (CVD).* CVD enables the fabrication of highly ordered structures for surface coating [10]. Typically, the surface to be coated is exposed to one or more volatile precursors, causing chemical reactions on and near the surface, which results in the deposition coating. The process is usually accompanied by the production of chemical by-products that are exhausted from the chamber along with unreacted precursor gases [55]. In recent years, many researchers used CVD to create highly-thermally-conductive ($3000 \text{ W m}^{-1} \text{ K}^{-1}$ to $5000 \text{ W m}^{-1} \text{ K}^{-1}$) [56] carbon nanotube (CNT) coatings to produce enhanced boiling surfaces. Fig. 4h shows a silicon surface coated by vertically aligned CNTs, which was synthesized by plasma enhanced chemical vapor deposition [57]. In some cases, CVD is combined

with other techniques for further modification. For example, Weibel et al. [58] further coated copper using physical vapor deposition on a CNT-coated copper surface to make it hydrophilic (Fig. 4i).

Other techniques such as additive machining (3D printing), epoxy binding, sputtering, evaporation, dripping and dipping are also reported in the literature. Detailed literature reviews on the current techniques for porous enhanced surfaces were recently provided by Patil and Kandlikar [59] and Leong et al. [10].

Compared to a structured surface, a porous surface has three important advantages: (i) in most cases, a porous matrix provides many more reentrant cavities thereby more activated nucleation sites; (ii) porous coatings can be made with a less expensive material than that required for base surface²; (iii) it is much easier to make micro/nano-scale structures on a porous surface. However, the structure of a porous surface cannot be manufactured to as precise a tolerance as a structured surface. In addition, the random porous structure is difficult to model, which makes the prediction of the boiling performance challenging. Porous surfaces are highly susceptible to oil fouling in refrigerant/lubricant boiling, which degrades heat transfer. For these reasons, the porous surface is reserved for use with clean fluids, such as process fluids, and not typically used commercially for refrigerant/lubricant mixtures.

2.3. Other surfaces

Wrapping a wire helically on a plain tube is a simple method for pool boiling heat transfer augmentation. Fig. 5a shows a typical wire-wrapped tube. The wrapping wire can enlarge the contact area between fluid and tube, and can also enhance bubble nucleation. The helical angle, pitch, diameter, and cross-section geometry of the wrapping wire play key roles in the heat transfer performance of wired-wrapped tubes [60,61].

² Care must be taken to avoid galvanic corrosion may be caused by contact between dissimilar metals in a conductive solution.

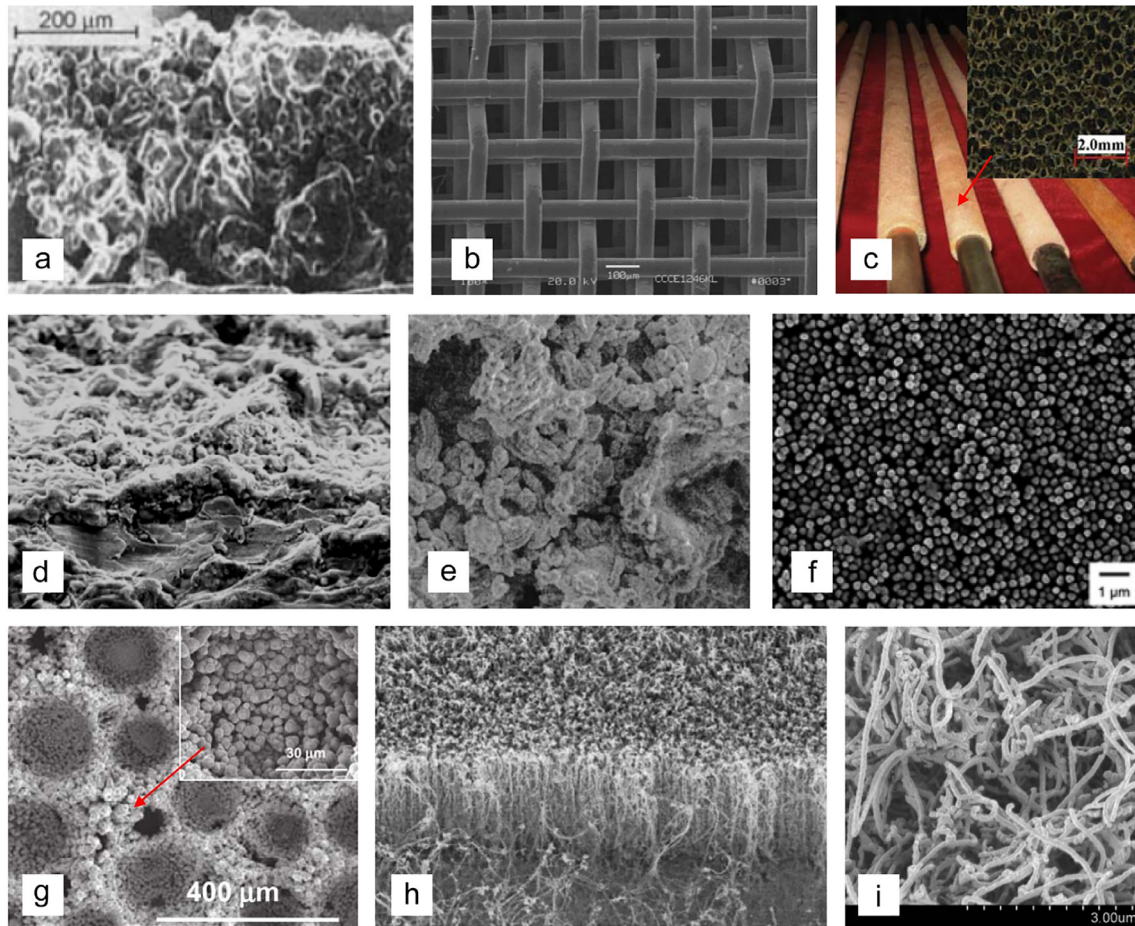


Fig. 4. Porous surfaces. (a) High-Flux tube (side view), from Chang and You [44]; (b) Cu surface coated by sintered Cu mesh (top view), from Li and Peterson [47]; (c) Cu tube coated by sintered Cu foam, from Ji et al. [48]; (d) Cu tube surface coated by Cu powders using flame spraying (top view), from Dewangan et al. [50]; (e) Cu tube surface coated by Mo using plasma spraying (side view), from Hsieh and Ke [51]. (f) Cu surface coated by Cu nanowires using electrochemical deposition (top view), from Yao et al. [53] (g) Structurally strengthened copper micro-porous coating made by electrochemical deposition (top view), from El-Genk and Ali [54]; (h) Si surface coated by CNTs using plasma enhanced chemical vapor deposition, from Ujereh et al. [57]; (i) Cu surface coated by CNTs using CVD and further coated by Cu using physical vapor deposition (top view), from Weibel et al. [58].

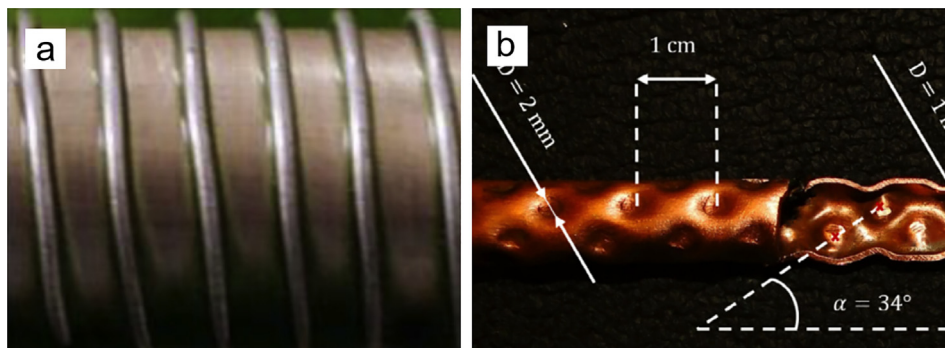


Fig. 5. Other surfaces. (a) Wire-wrapped tube, from Ali and Qasim [60]; (b) dimpled tube, from Shafae et al. [62].

The dimpled tube is a simple and a relatively inexpensive enhanced tube (Fig. 5b). Dimpled tubes are made from plain tubes by metal-forming dimples on the tube surface. The dimples can improve the heat transfer performance through a combination of increased turbulence, boundary layer disruption, secondary flow generation, and more nucleation sites [42]. The geometric parameters (shape, depth, pitch, diameter) and arrangement of dimples have significant effects on the overall performance [62].

3. Measurements for low-GWP refrigerants on enhanced surfaces

Tables 3, 4, and 5 chronologically summarize the existing literature for pool boiling measurements on enhanced surfaces for the low-GWP refrigerants: hydrofluoroolefin (HFO), hydrocarbon (HC), ammonia (NH_3), and carbon dioxide (CO_2). The literature is categorized by the enhanced surface type (structured, porous) in Tables 3

Table 3
Summary of pool boiling data of hydrofluoroolefin (HFO) refrigerants on enhanced surfaces.

| Authors & year | Low-GWP refrigerants | Features (or commercial name, if any) of enhanced surface | Base material, geometry | Heating method | Saturation condition | Heat flux [kW/m ²] | Uncertainty for HTC | HTC enhancement factor |
|----------------------------------|---|--|-------------------------|----------------|---|--------------------------------|---|--|
| <i>Structured surfaces</i> | | | | | | | | |
| Park and Jung (2010) [64] | R1234yf | Low fins (1023 fpm, $H_{fin} = 1.21$ mm) | Copper, flat | Electrical | $T_s = 7$ °C | 10–200 | <±4.4% | 1.6–3.0 |
| van Rooyen and Thome (2013) [67] | R1234ze(E) | Turbo-B5, GEWA-B5 | Copper, tubular | Fluid | $T_s = [5, 25]$ °C | 15–70 | Turbo-B5: <±30.73% GEWA-B5: <±40.57% | – |
| Lee et al. (2014) [68] | R1234yf | Turbo-B (1653 fpm, $H_{fin} = 0.44$ mm), Turbo-C (1653 fpm, $H_{fin} = 0.76$ mm), Thermoexcel-E (1928 fpm, $H_{fin} = 0.49$ mm) | Copper, flat | Electrical | $T_s = 7$ °C | 10–200 | <±6% | Turbo-B: 1.4–3.4 Turbo-C: 1.5–2.7 Thermoexcel-E: 1.1–5.0 |
| Gorgy (2016) [69] | R1234ze, R1233zd(E), R450A (R134a/R1234ze mixture, 42/58 by mass) | Turbo-ESP | Copper, tubular | Fluid | $T_s = 4.44$ °C | 10–110 | R1234ze: ±5% to ±18% R1233zd(E): ±5% to ±22% R450A: ±5% to ±18% | – |
| Nagata et al (2017) [70] | R1234ze(Z) | Enhanced tubes with different open-mouth width | Titanium, tubular | Fluid | $T_s = 10, 30, 60$ °C | 0.55–79.8 | – | 2–13 |
| Byun et al. (2017) [71] | R1234ze(E), R1233zd(E) | Enhanced tube #1 (similar to Turbo-B, 1575 fpm, $H_{fin} = 0.55$ mm); Enhanced tube #2 (similar to Turbo-BII, 2165 fpm, $H_{fin} = 0.61$ mm) | Copper, tubular | Fluid | $T_s = 4.4, 26.7$ °C | 10–50 | ±11% to ±47% | Enhanced tube #1: up to ~2.5 for R1234ze(E), up to ~2.3 for R1233zd(E); Enhanced tube #2: up to ~4.4 for R1234ze(E), up to ~6.6 for R1233zd(E). |
| Kedzierski et al. (2018) [72] | R1234yf, R513A (R1234yf/R134a, 56/44 by mass), R450A (R134a/R1234ze, 42/58 by mass) | Turbo-ESP (1928 fpm, $H_{fin} = 0.4$ mm) | Copper, flat | Fluid | $T_s = 277.6$ K | 10–120 | – | – |
| Kedzierski and Lin (2018) [73] | R1336mzz(Z) | Turbo-ESP (1928 fpm, $H_{fin} = 0.4$ mm) | Copper, flat | Fluid | $T_s = 277.6, 298.1, 318.1$ K | 10–120 | – | – |
| <i>Porous surfaces</i> | | | | | | | | |
| Moreno et al. (2013) [74] | R1234yf | Porous coating by modified copper powders: – fabricated by fusing at elevated temperature – coating thickness: ~150 μm. – coating porosity: (40–50)%. | Copper, flat | Electrical | $T_s = [25, 60]$ °C | 2–600 | <±4% | Up to ~4.5 |
| Koudou et al. (2017) [75] | R1234ze(E), R1234ze(Z) | Periodically line-patterned valleys covered with nano-sized lamellae: – fabricated by LISS – super-hydrophilic | Copper, flat | Electrical | For R1234ze(E), $P_s = [0.16, 0.20]$ MPa; for R1234ze(Z), $P_s = [0.42, 0.54]$ MPa | 20–1000 | – | – |

Table 4
Summary of pool boiling data of hydrocarbon (HC) refrigerants on enhanced surfaces.

| Authors & year | Low-GWP refrigerants | Features (or commercial names, if any) of enhanced surface | Base material, geometry | Heating method | Saturation condition | Heat flux [kW/m ²] | Uncertainty for HTC | HTC enhancement factor |
|--|----------------------------------|--|--------------------------|----------------|------------------------|--------------------------------|---|--|
| <i>Structured surfaces</i> | | | | | | | | |
| Hübner and Küstler (1997) [76] | R290 | Trapezoid-shaped fin tube (1417 fpm, $H_{fin} = 0.95$ mm); T-shaped fin tube (748 fpm, $H_{fin} = 1.04$ mm); Y-shaped fin tube (1024 fpm, $H_{fin} = 1.10$ mm) | Copper, tubular | Electrical | $p^* = [0.1, 0.8]$ | 0.02–20 | – | Trapezoid-shaped fin tube: up to ~1.5; T-shaped fin tube: up to ~2.5 Y-shaped fin: up to ~3.8 Up to 3 |
| Metz et al. (2001) [77] | R290 | PB1, PB2, PB3, PB4 | Carbon steel, tubular | Electrical | $T_s = [253, 293]$ K | 2–100 | – | Up to 4 |
| Mertz et al. (2002) [78] | R600a | PB1, PB2, PB3, PB4 | Carbon steel, tubular | Electrical | $T_s = [243, 293]$ K | 2–100 | – | Up to 3 |
| Kulenovic et al. (2002) [79] | R290 | PB4 | Copper, tubular | Electrical | $T_s = [243, 293]$ K | 2–100 | – | – |
| Chen et al. (2004) [80] | R290, R600a | PB1, PB4 | Carbon steel, tubular | Electrical | $P_s = [2.2, 8.4]$ bar | 0.2–20 | – | – |
| Chen et al. (2005) [81,82] | R290, R600a, R290/R600a mixtures | PB1 (2004 fpm, $H_{fin} = 0.694$ mm), PB2 (1912 fpm, $H_{fin} = 0.686$ mm), PB3 (1930 fpm, $H_{fin} = 0.679$ mm), PB4 (1966 fpm, $H_{fin} = 0.711$ mm) | Carbon steel, tubular | Electrical | $T_s = [243, 293]$ K | 1–100 | Smooth: $\pm 1.3\%$ to $\pm 10\%$ PB3: $\pm 10\%$ to $\pm 100\%$ | PB1: up to 1.8 PB2: up to 1.5 PB3: up to 12 PB4: up to 5 |
| Jung et al. (2005) [83] | R1270, R290, R600a, R600, RE170 | Low fin tube (1023 fpm); Turbo-B; Thermoexcel-E | Copper, tubular | Electrical | $T_s = 7$ °C | 10–80 | Low fin: $< \pm 6\%$ Turbo-B: $< \pm 14\%$ Thermoexcel-E: $< \pm 19\%$ | Low fin: 1.2–2.4 Turbo-B: 2.0–6.1 Thermoexcel-E: 2.3–9.4 |
| Kotthoff et al. (2006) [84] | R290 | (1) Macro-cavities with reduced-width mouth; (2) Macro-cavities without reduced-width mouth; | Copper, tubular | Electrical | $p^* = [0.05, 0.8]$ | 0.5–70 | – | With reduced-width mouth: up to 1.45; without reduced-width mouth: up to 1.35 4–10 |
| Luke and Müller (2010) [85] | R290 | GEWA-PB | Mild steel, tubular | Electrical | $p^* = [0.03, 0.5]$ | 0.05–100 | – | – |
| <i>Porous surfaces</i> | | | | | | | | |
| Zhou and Bier (1997) [86] | R290, R600a, R290/R600a mixtures | Porous coating of Al ₂ O ₃ to TiO ₂ ceramics – fabricated by plasma spraying – thickness: 0.2 mm | Copper, tubular | Electrical | $p^* = [0.1, 0.4]$ | 0.2–50 | – | – |
| Vasiliev et al. (1998) [87] | R290 | Porous coating of stainless steel layer: – fabricated by gas-thermal spraying – thickness: (0.1–0.3) mm – porosity: (4–17)% | Stainless steel, tubular | Electrical | $T_s = [-10, 40]$ °C | 0.1–100 | – | 3–5 for $q < 8$ kW/m ² ; 2.5–3 for $q > 8$ kW/m ² ; |
| Vasiliev et al. (2002) [44] | R290 | Porous coating of Copper powders (40–200 μm) – fabricated by sintering – thickness: (0.05–0.5) mm – porosity: (50–55)% | Copper, tubular | Electrical | $T_s = [-10, 30]$ °C | 0.1–120 | – | 3–5 |
| Hsieh and Yang (2001) [88] | R600a | (1) Porous coating of Copper powders: – fabricated by plasma spraying – thickness: 0.3 mm – porosity: 0.055 – mean pore diameter: 3 μm (2) Porous coating of Mo powders: – fabricated by plasma spraying – thickness: 0.1 mm – porosity: 0.057 – mean pore diameter: 4 μm | Copper, tubular | Electrical | $T_s = 18$ °C | 0.6–30 | $< \pm 10.8\%$ for $q = 0.6$ kW/m ² ; $< \pm 3.48\%$ for $q = 30$ kW/m ² ; | Copper porous coating: up to 2.01; Mo porous coating: up to 1.63 |
| Dewangan et al. (2016–2017) [50,89,90] | R600a | Porous coating of copper powders: – fabricated by gas flame spraying – thickness: (42.2–271.4) μm – porosity: (8.5–13.8)% – mean pore diameter: (1.75–2.58) μm | Copper, tubular | Electrical | $T_s = 10$ °C | 5–50 | $< \pm 11\%$ | Up to ~2 |

Table 5
Summary of pool boiling data of ammonia (NH₃) and carbon dioxide (CO₂) on enhanced surfaces.

| Authors & year | Low-GWP Refrigerant | Features (or commercial names, if any) of enhanced surface | Base material, geometry | Heating method | Saturation condition | Heat flux [kW/m ²] | Uncertainty for HTC | HTC enhancement factor |
|------------------------------------|--|---|--------------------------|----------------|----------------------------------|--------------------------------|---------------------|---|
| Djundin et al. (1984) [91] | NH ₃ | (1) Porous aluminum layer: - thickness: 0.3 mm - porosity: 29% - equivalent pore diameter: 37 μm (2) Grooves made by vibrorolling - width: 1.5 mm - depth: 1.0 mm (3) Fluorocarbon coating - thickness: 50 μm Aluminum porous coating: - thickness: 0.26–1.0 mm - porosity: (25–44.1)% - equivalent pore diameter: (24.1–40.1) μm Structured reentrant channels Integral-fin tube (1260 fpm, H _{fin} = 0.9 mm) | Steel, tubular | - | T _s = [263, 293] K | 2–25 | - | (1) Porous aluminum layer 1.4 (2) Vibrorolling grooves: 1.3–1.6 (3) Fluorocarbon coating: 4–5 |
| Daniłova et al. (1990) [93] | NH ₃ | | Steel, tubular | - | T _s = [253, 293] K | 2–25 | - | 2–5 |
| Zheng et al. (2008) [94] | NH ₃ /PAG oil mixture (oil mass fraction 0–10%) | | Carbon steel, tubular | Fluid | T _s = [-23.3, 7.2] °C | 10–60 | ±10% to ±15% | - |
| Fernández-Seara et al. (2016) [95] | NH ₃ | | Titanium, tubular | Fluid | T _s = [4, 10] °C | 3–60 | (±1.6 to ±10.5)% | 1–1.3 |
| Liu et al. (2016) [96] | CO ₂ | Three different screwed (integral-fin) tubes (E1, E2, E3) | Stainless Steel, tubular | Electrical | P _s = [2, 4] MPa | 10–50 | <±14.97% | E1: 1.5–1.72 E2: 1.6–1.82 E3: 2–2.2 |

and 4, but not done so in Table 5 because significantly fewer measurements with NH₃ and CO₂ were found. Tables 3, 4, and 5 use the same columns. Column 1 gives the reference information of each literature. Column 2 lists only the low-GWP refrigerants that were tested. Column 3 briefly describes the surface features (or commercial names, if any) of the tested enhanced surfaces and fabrication techniques for porous test surfaces and fins-per-meter (fpm) for structured surfaces. Column 4 lists the base surface material and its geometry (tubular or flat). Column 5 indicates whether the heating boundary condition was achieved by fluid or electrical heating. The significance of column 5 is that Kedzierski [36] has shown that the pool-boiling heat flux achieved by fluid heating can be as much as 32% larger than an electrically obtained heat flux for the same boiling superheat. Darabi et al. [63] have shown a similar heating boundary condition effects for flow boiling. Columns 6–9 list the saturation condition (the saturation temperature or the pressure, or the reduced pressure), the heat flux, the uncertainty of the HTC, and the enhancement factor, respectively. The HTC enhancement factor (F_E) is defined as the ratio of the HTC of the enhanced surface to the HTC of the plain surface, which is either directly given by the literature or estimated from the data in the literature. The HTC enhancement factor could not be obtained from some studies due to the lack of the plain surface data. The reviewed literature is introduced in detail in the following subsections.

3.1. Hydrofluoroolefins

- Structured surface

In 2010, Park and Jung [64] measured the pool boiling of R1234yf on a plain and several low fin surfaces. The experiments were conducted at a saturation temperature of 7 °C and a range of heat fluxes from 10 kW/m² to 200 kW/m². The investigated surface was a square, flat, copper plate (9.53 mm × 9.53 mm) with nine 1.21 mm-high fins, simulating the 1023 fpm low-fin tube. The boiling HTC for R1234yf on the low-fin surface was about 1.6–3.0 times that of a plain surface. The authors also concluded that the nucleate boiling characteristics of R1234yf were similar to those of R134a. In addition, they compared the nucleate boiling HTCs of R1234yf and R134a on a plain surface to the correlations developed by Jung et al. [65] and Gorenflo et al. [66]. For both R134a and R1234yf, the correlations by Jung et al. [65] and Gorenflo et al. [66] deviated from the measurements by 12.7% and 9.4%, respectively, for heat fluxes less than 200 kW m⁻². Thus, the conventional correlations could be used for R1234yf.

Van Rooyen and Thome [67] measured the pool boiling HTC for R1234ze(E) outside two commercial enhanced tubes, the Turbo-B5 and the Gewa-B5, at a saturation temperatures between 5 °C and 25 °C and a heat flux between 15 kW/m² and 70 kW/m². The pool boiling HTC of R1234ze(E) ranged between 25 kW/(m² K) and 31 kW/(m² K) on the Turbo-B5, and between 20 kW/(m² K) and 44 kW/(m² K) on the GEWA-B5. They found that the HTC was significantly affected by heat flux, but slightly affected by the tube type and the saturation temperature.

Lee et al. [68] measured the pool boiling HTC of R1234yf for a plain surface and for three enhanced surfaces: the Turbo-B, the Turbo-C, and the Thermoexcel-E. The studied surfaces were square copper plates with the same dimensions as those of [64]. The tests were conducted at a saturation temperature of 7 °C and for heat fluxes between 10 kW/m² and 200 kW/m². They reported that the Thermoexcel-E surface exhibited the best heat transfer performance (with the enhancement factor up to 5) for heat fluxes less than 150 kW/m², while the Turbo-B and the Turbo-C surfaces were marginally better at heat fluxes larger than 150 kW/m². Thus, they concluded that the Thermoexcel-E was suitable for low heat flux

refrigeration and air-conditioning applications, while the Turbo-B and the Turbo-C surfaces were suitable for high heat flux applications such as electronic cooling.

Gorgy [69] studied the pool boiling heat transfer of R1234ze(E), R1233zd(E), and R450A on a highly enhanced tube (Turbo-ESP). The pool boiling experiments were conducted at a saturation temperature of 4.4 °C and for a range of heat fluxes between 10 kW/m² and 110 kW/m². Under the studied conditions, the HTC of R1234ze(E), R1233zd(E), and R450A on the Turbo-ESP were between (25 and 28) kW/(m² K), (17 and 27) kW/(m² K), and (14 and 25) kW/(m² K), respectively. Plain tube data for these refrigerants were not reported.

Nagata et al. [70] measured the pool boiling heat transfer for R1234ze(Z) on a plain tube and three enhanced titanium tubes. The depth and the inner width of the reentrant cavities of the enhanced tubes ranged from 0.375 mm to 0.410 mm and from 0.270 mm to 0.310 mm, respectively. The tests were conducted at saturation temperatures from 10 °C to 60 °C and heat fluxes from 0.55 kW/m² to 79.8 kW/m². The HTC enhancement produced by the enhanced tubes was from 2 to 13 over the entire test range. The study showed that the opening width of the reentrant cavity had a significant effect on the HTC enhancement. At lower saturation temperatures and heat fluxes, the enhanced tubes with the narrowest openings exhibited the highest HTC; while at greater saturation temperatures and heat fluxes, the enhanced tubes with the widest openings had the highest HTC.

Byun et al. [71] investigated the pool boiling performance of R1234ze(E) and R1233zd(E) on a plain tube and two internally and externally enhanced tubes (#1, #2). The external surface of the Enhanced tube #1 was similar to that of the Turbo-B, while that of the Enhanced tube #2 is similar to that of Turbo-BII. The experiments were performed for saturation temperatures between 4.4 °C and 26.7 °C and for heat fluxes between 10 kW/m² and 50 kW/m². As shown in Fig. 6, the maximum enhancement factor of the Enhanced tube #1 was about 2.5 for R1234ze(E) and 2.3 for R1233zd(E), while that of the Enhanced tube #2 was about 4.4 for R1234ze(E) and 6.6 for R1233zd(E). In particular, the HTC of R1233zd(E) on the Enhanced tube #2 was relatively large compared with other tubes, which was attributed to the shape of the tube surface.

Kedzierski et al. [72] measured the pool boiling heat transfer of R1234yf, R513A (R1234yf/R134a (56/44 by mass)), and R450A (R134a/R1234ze (42/58 by mass)), which are the replacement refrigerants for R134a, on a flattened, horizontal Turbo-ESP surface. The measurements were performed at saturation temperature of approximately 4.4 °C and for a range of heat fluxes between 10 kW/m² and 110 kW/m². For fixed wall superheat, the authors showed that the measured boiling heat flux for R134a was larger than that measured for the proposed replacement refrigerants for heat fluxes greater than 20 kW/m². On average, the heat flux for R1234yf and R513A were 16% and 19% less than that for R134a, respectively, for R134a heat fluxes between 20 kW/m² and 110 kW/m². The heat flux for R450A was, on average, 57% less than that of R134a for heat fluxes between 30 kW/m² and 110 kW/m².

More recently, Kedzierski and Lin [73] measured a novel HFO refrigerant for heat recovery and air-conditioning applications, R1336mzz(Z), on a flattened, horizontal Turbo-ESP surface for heat fluxes between roughly 10 kW/m² and 120 kW/m². The study showed that the boiling performance of R1336mzz(Z) on the TurboESP did not differ statistically from that of R123 for heat fluxes between 13 kW/m² and 59 kW/m². For heat fluxes larger than 59 kW/m², the R123 boiling heat flux was up to 5% larger than the heat flux for R1336mzz(Z). For heat fluxes between 4 kW/m² and 13 kW/m², the R123 heat flux was approximately 53% larger than that of R1336mzz(Z). The R1336mzz(Z) pool boiling curve was measured for three saturation temperatures and exhibited

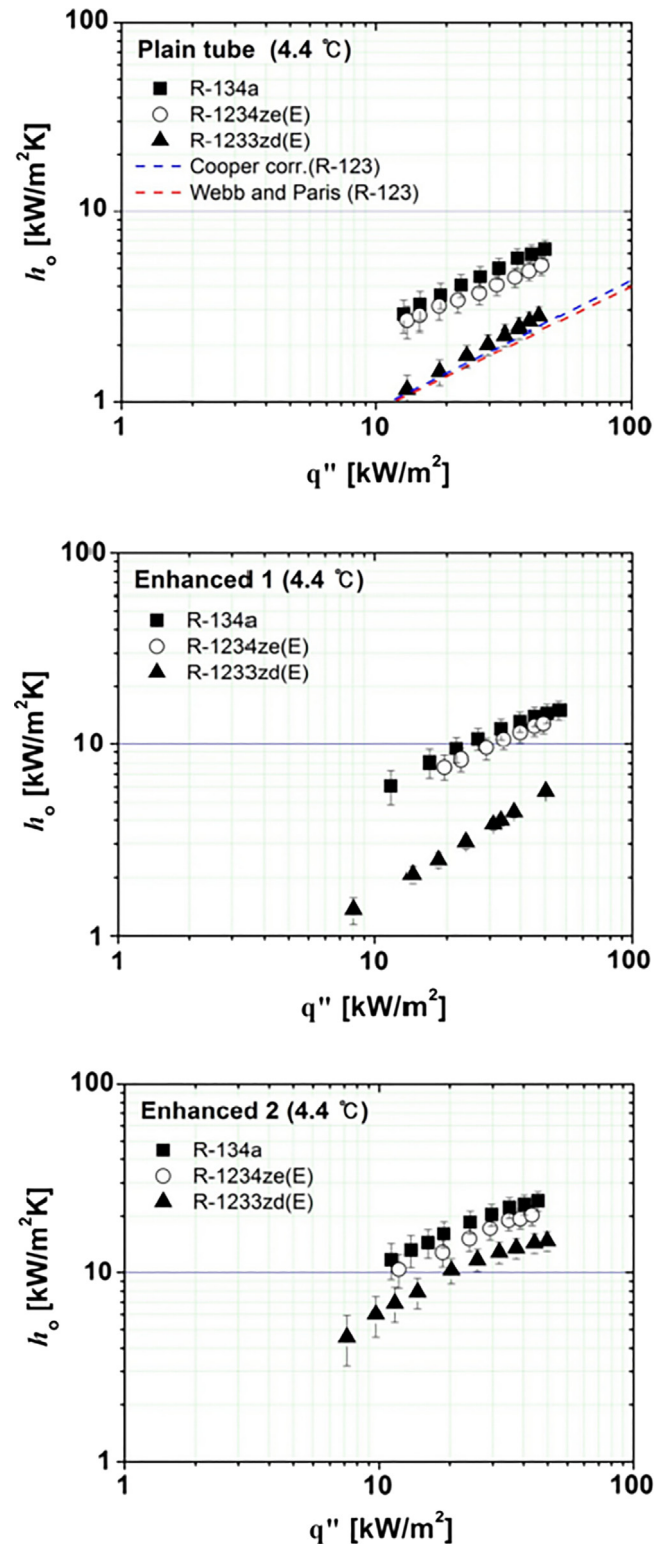


Fig. 6. Pool boiling HTCs of R1234ze(E) and R1233zd(E) on plain and two enhanced tubes. (from Byun et al. [71]).

an optimum with respect to saturation temperature near the middle saturation temperature of 298.1 K.

– Porous surface

Moreno et al. [74] studied the pool boiling performance of R1234yf on a plain and on a microporous-coated surfaces for

saturation temperatures between 25 °C and 75 °C and for heat fluxes up to 600 kW/m². The coating was 150 μm thick with a porosity between 40% and 50%, made by fusing copper particles onto a copper surface at elevated temperature. The porous surface exhibited significant enhancement of the HTC compared to the plain surface with the enhancement factor up to 4.5 which was achieved at saturation temperature of 40 °C and heat flux of approximately 30 kW/m².

Kondou et al. [75] fabricated a microporous surface using Laser Interference Surface Structuring (LISS) technique, and measured the boiling curves of R1234ze(E) and R1234ze(Z) on this surface. The LISS technique employs two or more overlapping laser beams to form unique intensity distributions with periodicities on the micron and sub-micron scale. The high-power laser modifies materials through photo-thermal interaction imparting its dual size characteristic to the material. The fabricated surface had a microstructure of periodically line-patterned valleys covered by nano-sized lamellae making it super-hydrophilic. As observed by the authors, the microporous surface exhibited the hysteresis of nucleate boiling inception for heat fluxes below 150 kW/m²; when the heat flux exceeded 150 kW/m², the wall superheat was significantly decreased by the microporous surface for both refrigerants.

– Summary

For HFO boiling studies, R1234yf is the most investigated refrigerant. Fig. 7 provides a summary of the R1234yf HTC enhancement factors (F_E) versus heat flux for the various studies and enhanced surfaces reviewed here. The F_E data in Fig. 7 were either directly given by the literature or estimated from the literature data. The retained range for the F_E data was for heat fluxes between approximately 10 kW/m² to 100 kW/m², which is the typical range for refrigeration and air-conditioning applications. As shown in Fig. 7, the Thermoexcel-E tube gave the best HTC enhancement (with F_E up to 5) for R1234yf for heat fluxes less than 30 kW/m², while the porous copper tube was better at medium to high heat fluxes (greater than 30 kW/m²).

The available data for other HFO refrigerants and their blends are still limited. For R1234ze(E), the enhanced tube #2 made by Byun et al. [71] (similar to Turbo-BII, 2165 fpm, $H_{fin} = 0.61$ mm) gave the best HTC enhancement (with F_E up to approximately 4.4). The enhanced tube #2 made by Byun et al. [71] also gave the best HTC enhancement (with F_E up to approximately 6.6) for R1233zd(E).

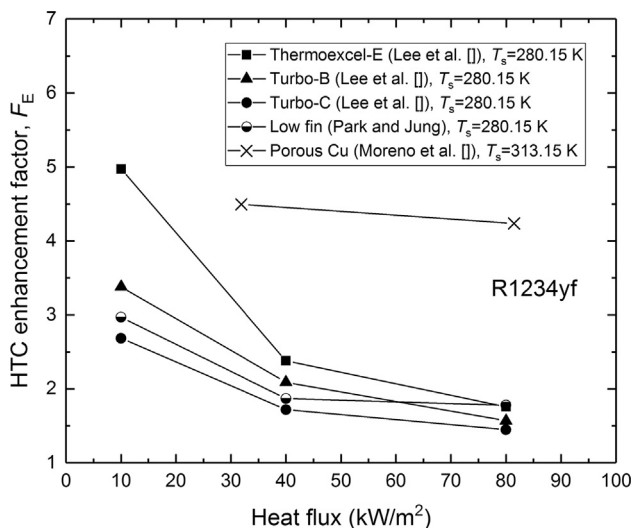


Fig. 7. R1234yf HTC enhancement factor (F_E) by different enhanced surfaces versus heat flux.

3.2. Hydrocarbon

– Structured surface

In 1997, Hübner and Küstler [76] measured the pool boiling HTC of R290 on a plain and three finned tubes (trapezoid-shaped, T-shaped and Y-shaped). The measurements were carried out at reduced pressures between 0.1 and 0.8 and for heat fluxes between 0.02 kW/m² and 20 kW/m². Compared to plain tubes, the boiling heat transfer on the enhanced tube with the trapezoid-shaped fins was considerably improved, and even better results were achieved with T-shaped or Y-shaped fins. The maximum HTC enhancement factors for the fins in trapezoid-shape, T-shape, and Y-shape were 1.5, 2.5, and 3.8, respectively.

Mertz et al. [77,78] measured R290 and R600a pool boiling on four enhanced tubes having nominally 2000 fpm and T-shaped fins with heights of approximately 0.7 mm forming reentrant cavities. Fig. 8 shows the carbon steel tubes as PB1, PB2, PB3, and PB4. The primary geometrical difference between the tubes was the treatment of the top of the finned surface, which were serrated to differing degrees causing a variation in the cavity openings for the fins. On average, the cavity openings for the PB1, PB2, PB3, and PB4 surfaces were 0.164 mm, 0.081 mm, 0.076 mm, and 0.062 mm, respectively. The saturation temperature ranged between –30 °C and 20 °C, and the heat fluxes ranged between 2 kW/m² and 100 kW/m². Mertz et al. [77,78] reported that the tube PB4 exhibited the best performance of the four tubes for both R290 and R600a. For R290, the largest HTC was 22 kW/(m² K), about 3 times that of the plain tube. For R600a, the highest HTC was 14 kW/(m² K), roughly 4 times of that of plain tube. Kulenovic et al. [79] also investigated the boiling of R600a on the tube PB4 with a high-speed video system and a digital image processing technique to record the bubble dynamics. The bubble departure diameter, the bubble generation frequency, and the flow velocity were measured for two heat fluxes: 2.2 kW/m² and 5 kW/m². Chen et al. [80] added to the bubble dynamics data for R600a and the PB4 tube by measuring more bubble parameters (such as active site density) to comprehensively describe the bubble growth process. In addition, Chen et al. [80] extended the experiments to include R290 and the PB1 tube and a plain tube. According to their bubble data, a larger heat transfer rate occurred for the enhanced tube, despite it having a lower active site density and nearly the same bubble frequency of the plain tube, because the enhanced tube had a significantly larger bubble departure diameter as compared to the plain tube. Chen et al. [80] proposed that the latent heat transfer was the dominant mechanism for the heat transfer enhancement on the reentrant surface, and the latent heat enhancement was mainly due to the evaporation of a thin liquid film inside the channels.

Chen et al. [81] measured the pool boiling heat transfer of R290, R600a, and three R290/R600a mixtures on the PB1–PB4 tubes using the same test rig and conditions as their previous studies [77–80]. Fig. 9 shows the measured HTC enhancement factor (F_E , ratio of enhanced surface HTC to plain surface HTC) for the four enhanced tubes. As shown in Fig. 9, the PB1 has a relatively large F_E for R290 (peaking between 1.5 and 2), but a small F_E for R600a (between 0.75 and 1) and their mixtures (between 0.3 and 1). Fig. 9 shows that the relative ranking of the F_E for the test fluids on the PB1 surface differs from that for the PB2, PB3, and PB4 surfaces. For example, the mixture boiling performance exceeds pure component performance for certain heat fluxes for the PB2 and the PB3 surfaces. This seemingly erratic mixture boiling performance was not explained by Chen et al. [81]. Fig. 11 also shows that the F_E for I-Butane on the PB3 surface was as large as approximately 12, while never exceeding 5 for the other surfaces for similar heat fluxes. The anomalously large F_E for I-Butane on the PB3 is likely

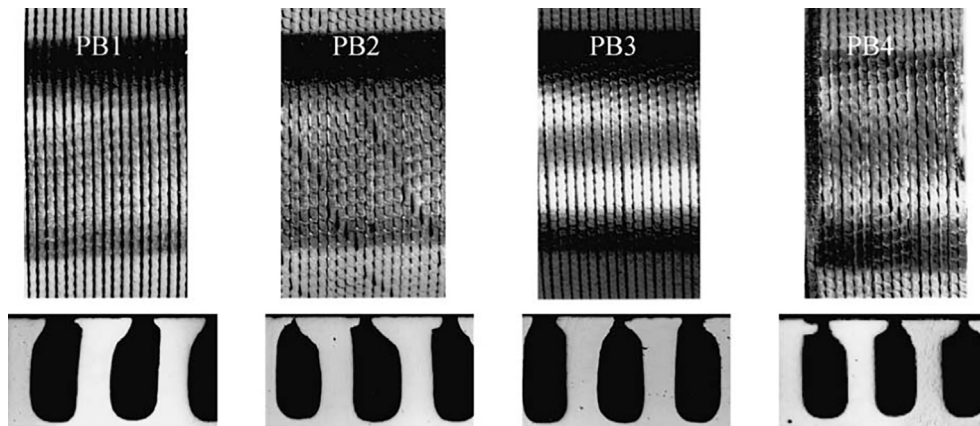


Fig. 8. Geometries of PB1, PB2, PB3 and PB4. (from Chen et al. [82]).

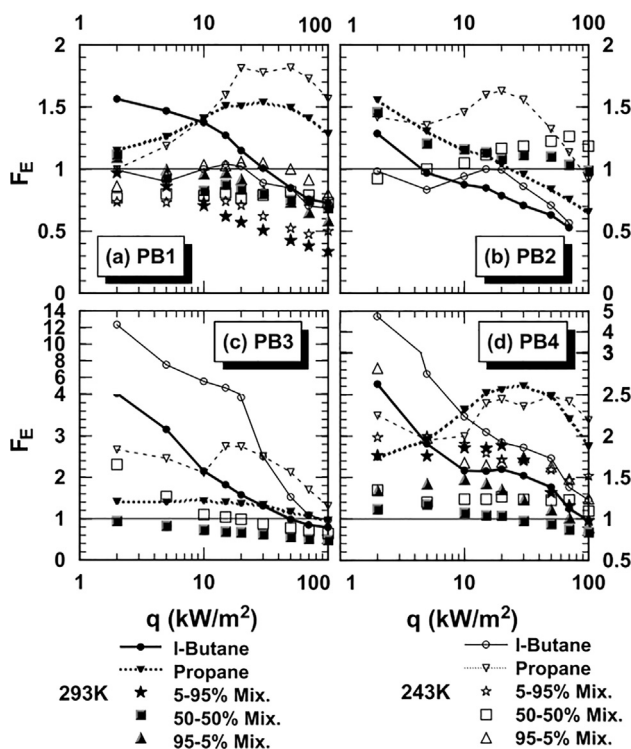


Fig. 9. Pool boiling enhancement factor (F_E) of PB1, PB2, PB3 and PB4 for R600a, R290 and their mixtures. (from Chen et al. [82]).

associated with the larger uncertainties in the measured superheat at low heat fluxes as stated in Chen et al. [82]. Because of the erratic mixture boiling performance, the exceedingly large F_E for I-Butane and the electrically obtained heat flux boundary condition, the reader should use these measurements with caution. In their accompanying paper, Chen et al. [82] visually studied the bubble behavior and explored the enhancement mechanism of R290, R600a, and the two mixtures for only the PB4 and the PB2 tubes. Consequently, the cause of the $F_E = 12$ enhancement on the PB3 surface was not explored beyond a possible large measurement uncertainty. The visual observation indicated a strong mixture effect on the nucleation and evaporation processes on the reentrant tubes, which was attributed to Marangoni convection. Chen et al. [82] found that typically the large-opening channels were more likely to be flooded at low heat flux, while small-opening channels were more likely to be clogged by vapor at high heat flux which deteriorates the heat transfer performance; thus, a surface

having moderate size with connected pores was favored for enhanced boiling.

Jung et al. [83] measured the boiling heat transfer of four hydrocarbon refrigerants (R1270, R290, R600a, and R600), and one ether (RE170)³ for three commercial enhanced tubes (low-fin tube, Turbo-B, and Thermoexcel-E) at a saturation temperature of 7 °C and for heat fluxes between 10 kW/m² and 80 kW/m². The measured HTC are shown in Fig. 10. Among these tubes, the Thermoexcel-E tube shows the best performance with the enhancement factor between 2.3 and 9.4 due to its sub-surface channels and reentrant cavities. The Turbo-B tube presents the enhancement factor ranging from 2.0 to 6.1. The low-fin tube shows a relatively lower enhancement factor ranging between 1.2 and 2.4. Jung et al. [83] also found that the enhancement factor for the HC refrigerants were up to 40% greater than those of HFC refrigerants for low heat fluxes, but exhibited similar ones for high heat fluxes.

Kotthoff et al. [84] experimentally studied heat transfer and bubble formation for R290 pool boiling on tubes with and without macro-cavities. Two types of macro-cavities were used: one was the “main structure” that had a reduced active cavity opening, and the other was the “secondary structure” that had a full cavity opening. The boiling tests were conducted for reduced pressures from 0.05 to 0.8, and for heat fluxes ranging from 0.5 kW/m² to 70 kW/m². The overall improvement of the average HTC achieved by the macro cavities was as large as 45% for the “main structure” and up to roughly 35% for the “secondary structure.” Luke and Müller [85] tested R290 on a mild steel GEWA-PB enhanced tube and on a plain tube for reduced pressures between 0.05 and 0.5 and for heat fluxes between 0.05 kW/m² and 100 kW/m², which covered most pool boiling regimes. The HTC enhancement factor varied from approximately 4 to 10 for heat fluxes of 100 kW/m² and 0.1 kW/m², respectively.

– Porous surface

Zhou and Bier [86] studied the pool boiling heat transfer of R290, R600a, and their mixtures on a horizontal copper tube coated with 0.2 mm thick Al₂O₃ and TiO₂ ceramics. The experiments were conducted at reduced pressure between 0.1 and 0.4, and for heat fluxes between 0.2 kW/m² and 50 kW/m². They showed that the HTCs of the ceramic-coated tube were as high as those of a sand-blasted tube with similar roughness for reduced pressures larger than 0.1, and even higher at lower reduced pressures. Also, the ceramic coatings were found to facilitate nucleation, which compensated for the insulating effect of low thermal conductivity of

³ The literature, on occasion, incorrectly categorizes RE170 as a hydrocarbon.

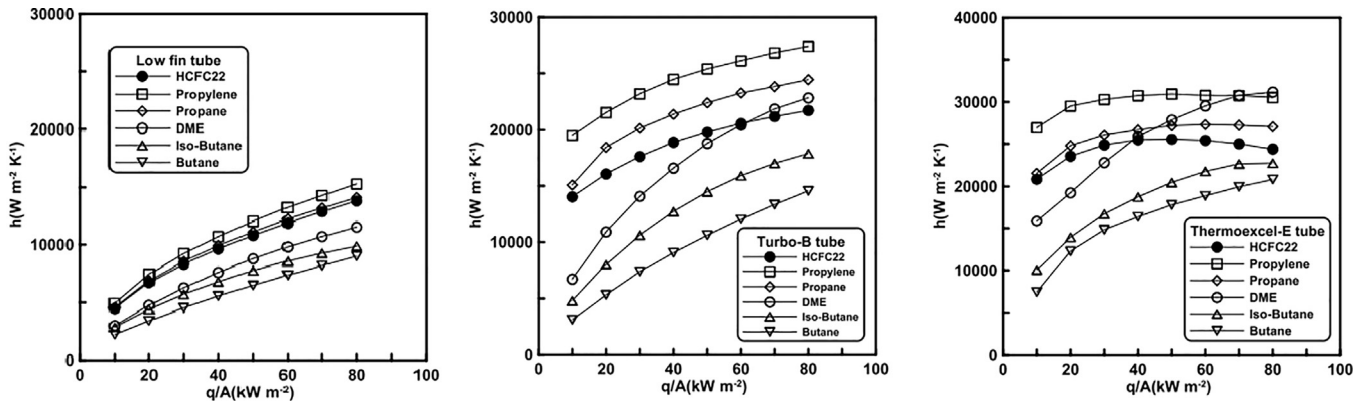


Fig. 10. Pool boiling HTCs of R1270, R290, R600a, R600, and RE170 on (a) low fin tube, (b) Turbo-B tube, and (c) Thermoexcel-E tube. (from Jung et al. [83]).

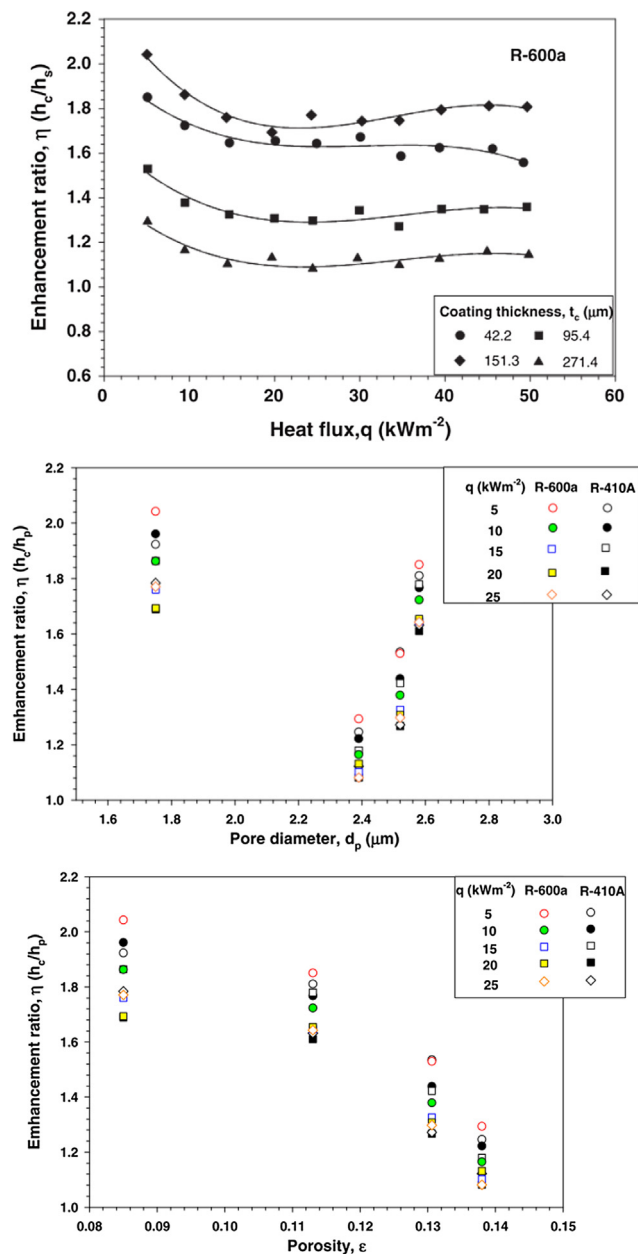


Fig. 11. Effects of coating thickness, pore size and porosity on pool boiling heat transfer. (from Dewangan et al. [50,89,90]).

ceramics. Nucleation enhancement was especially prevalent for mixtures.

Vasiliev et al. [87] tested the heat transfer of R290 during pool boiling on plain and on porous-coated stainless steel tubes at saturation temperatures between $-10\text{ }^{\circ}\text{C}$ and $40\text{ }^{\circ}\text{C}$ and for heat fluxes between 0.1 kW/m^2 and 100 kW/m^2 . The porous coating was made of stainless steel using the gas-thermal spraying technique. The coating thickness ranged from 0.1 mm to 0.3 mm , and the porosity ranged from 4% to 17% . The maximum HTC enhancement factor was approximately 3, which was observed for a coating thickness of 0.2 mm and a porosity of 12.5% .

Vasiliev et al. [44] tested R290 pool boiling on a copper tube sintered with a copper powder. The tests were performed at saturation temperatures between $-10\text{ }^{\circ}\text{C}$ and $30\text{ }^{\circ}\text{C}$ and for heat fluxes between 0.1 kW/m^2 and 120 kW/m^2 . The coating thickness was varied from 0.05 mm to 0.5 mm , and the powder diameter was varied from $40\text{ }\mu\text{m}$ to $200\text{ }\mu\text{m}$. The HTCs for the porous-coated tubes were up to $30\text{ kW}/(\text{m}^2\text{ K})$; roughly 3–5 times that of a plain tube. Vasiliev et al. [44] suggested that the mean pore hydraulic dimension was the key parameter for determining the heat transfer performance of the porous-coated surface.

Hsieh and Yang [88] measured the pool boiling HTC of R600a on a plain tube and on two porous tubes coated by Cu and Mo. The experiments were conducted at a saturation temperature of $18\text{ }^{\circ}\text{C}$ and for heat fluxes between 0.6 kW/m^2 and 30 kW/m^2 . The maximum HTC enhancement, approximately 1.7, occurred for the Cu porous-coated tube at a heat flux of 6 kW/m^2 . Hsieh and Ke [51] observed and quantified the boiling bubble dynamics. They found that the nucleation site density for the porous-coating was remarkably greater than that of the other surfaces and that it was a linear function of the heat flux.

Recently, Dewangan et al. [50,89,90] investigated the effects of coating thickness, pore size, and porosity on the heat transfer enhancement for porous-coated tubes (see Fig. 11). Four porous-coated tubes were fabricated by flame spraying copper powders onto copper tubes with various manufacturing parameters. Boiling tests with the porous-coated tubes and a plain tube were done with R600a for a fixed saturation temperature of $10\text{ }^{\circ}\text{C}$ and for heat fluxes between 5 kW/m^2 to 50 kW/m^2 . They showed that the coating with medium thickness ($151.3\text{ }\mu\text{m}$) and the smallest pore diameter ($1.75\text{ }\mu\text{m}$) gave the highest HTC enhancement factor (about 2), while the largest porosity produced the smallest enhancement.

– Summary

The existing measurements on HC refrigerants mainly focus on R290 and R600a. Figs. 12 and 13 summarize the effect of heat flux

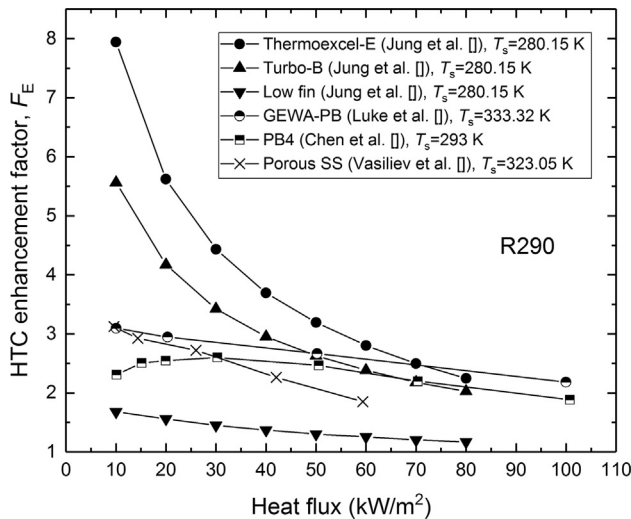


Fig. 12. R290 HTC enhancement factor (F_E) by different enhanced surfaces versus heat flux.

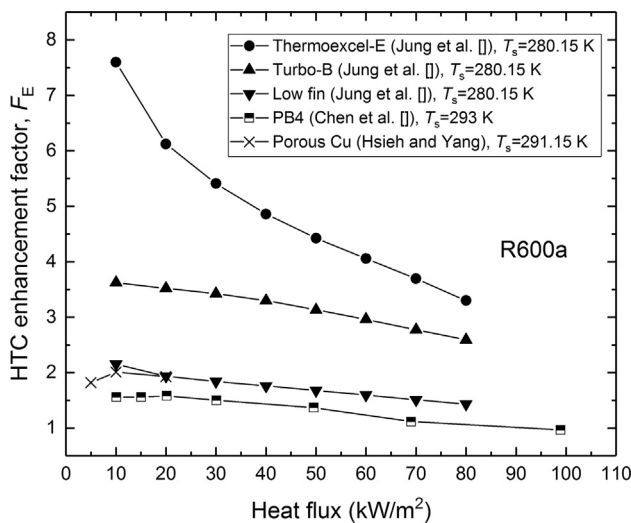


Fig. 13. R600a HTC enhancement factor (F_E) by different enhanced surfaces versus heat flux.

on the reviewed HTC enhancement factors (F_E) for R290 and the R600a, respectively. As done previously, the retained range for the F_E data was for heat fluxes between approximately 10 kW/m² to 100 kW/m². As shown by Fig. 12, the Thermoexcel-E tube gave the best HTC enhancement (with F_E up to 8) for R290 at heat fluxes less than 70 kW/m². For heat fluxes greater than 70 kW/m², the Thermoexcel-E, Turbo-B, GEWA-PB, and PB4 showed comparable HTC enhancements with F_E of approximately 2.2. For R600a, as shown by Fig. 13, the Thermoexcel-E tube gave the best HTC enhancement with F_E up to approximately 7.6. The available data for other HC refrigerants and their blends are still very limited. According to the measurements by Jung et al. [83] (Fig. 10), the Thermoexcel-E tube also gave the best HTC enhancements for R1270, R600, and RE170, with F_E up to approximately 8.4, 8.1, and 8.9, respectively.

3.3. Ammonia and carbon dioxide

Djundin et al. [91] investigated the effect of various surface enhancements on the pool boiling performance of ammonia. They

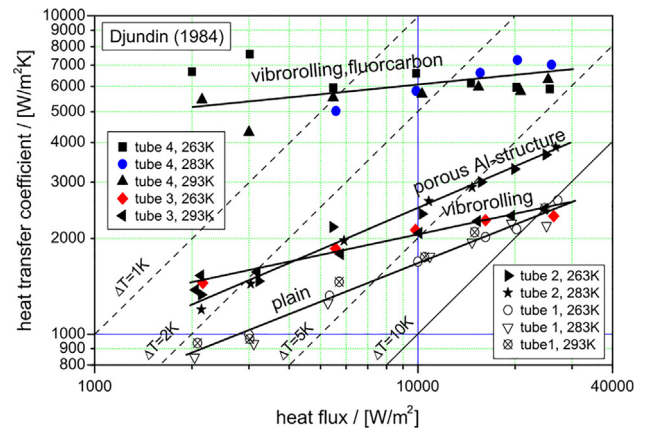


Fig. 14. Pool boiling heat transfer of NH₃ on surfaces with vibrorolling grooves, porous aluminum structure, and fluorocarbon coating (from Spindler [92]).

tested a plain tube, a tube with an aluminum porous layer (thickness: 0.3 mm; porosity: 29%; equivalent pore diameter: 37 μm), a tube having grooves made by vibrorolling (width 1.5 mm, depth 1.0 mm), and a tube coated with a fluorocarbon layer (thickness: 50 μm). The saturation temperatures for testing ranged from 263 K to 293 K, and the heat fluxes varied from 2 kW/m² to 25 kW/m². Fig. 14 shows the measured HTC for ammonia on these tubes, re-plotted by Spindler [92]. The HTC enhancement factor for the aluminum porous-coated tube was as large as 1.4, while that for the grooved tube was about 1.6 for a heat flux of 0.1 kW/m² and decreased for increasing heat flux. The fluorocarbon coated tube yielded a significantly larger enhancement factor, which was as large as 5.

Danilova et al. [93] measured the pool boiling HTCs of ammonia on various aluminum porous-coated tubes. The coating thickness varied from 0.26 mm to 1.0 mm, the porosity ranged from 25% to 44.1%, and the equivalent pore diameter varied from 24.1 μm to 40.1 μm. The tests were performed between saturation temperatures of 253 K and 293 K, and for heat fluxes between 2 kW/m² to 25 kW/m². The authors showed that the aluminum porous coated tube yielded a HTC enhancement factor between 2 and 5 for the test conditions.

Zheng et al. [94] studied the influence of lubricant on the pool boiling of ammonia for a structured surface with reentrant channels. An evaporator containing a bundle of enhanced tubes served as the heat transfer test apparatus. The polyalkylene glycol (PAG) lubricant mass fraction was varied from 0% to 10%. The tests were conducted at saturation temperature between −23.3 °C and 7.2 °C and for heat fluxes between 10 kW/m² and 60 kW/m². The measured HTCs were compared to the HTC for a single tube. Zheng et al. [94] showed that the addition of lubricant reduced the performance of the enhanced tube, while increasing the performance of the plain tube.

Fernández-Seara et al. [95] experimentally studied pool boiling of ammonia on a 1260 fpm integral-fin tube. The test saturation temperatures for pool boiling were 4 °C, 7 °C, and 10 °C. The HTCs were collected for the heat fluxes between 3 kW/m² and 60 kW/m². Their measured HTC enhancement factor varied from 1 to 1.3 and was nearly independent of heat flux or saturation temperature. The weak relationship between the enhancement and the heat flux was confirmed by the boiling photographs shown in Fig. 15. In Fig. 15, the size and the quantity of the bubbles on the integral-fin tube and on the plain tube were similar at high heat fluxes, suggesting that the enhancement for the integral-fin tube is mainly due to the extended surface area. Fig. 15 also shows that the integral-fin tube exhibits a greater delay in incipient nucleation with respect to heat flux as compared to the plain tube.

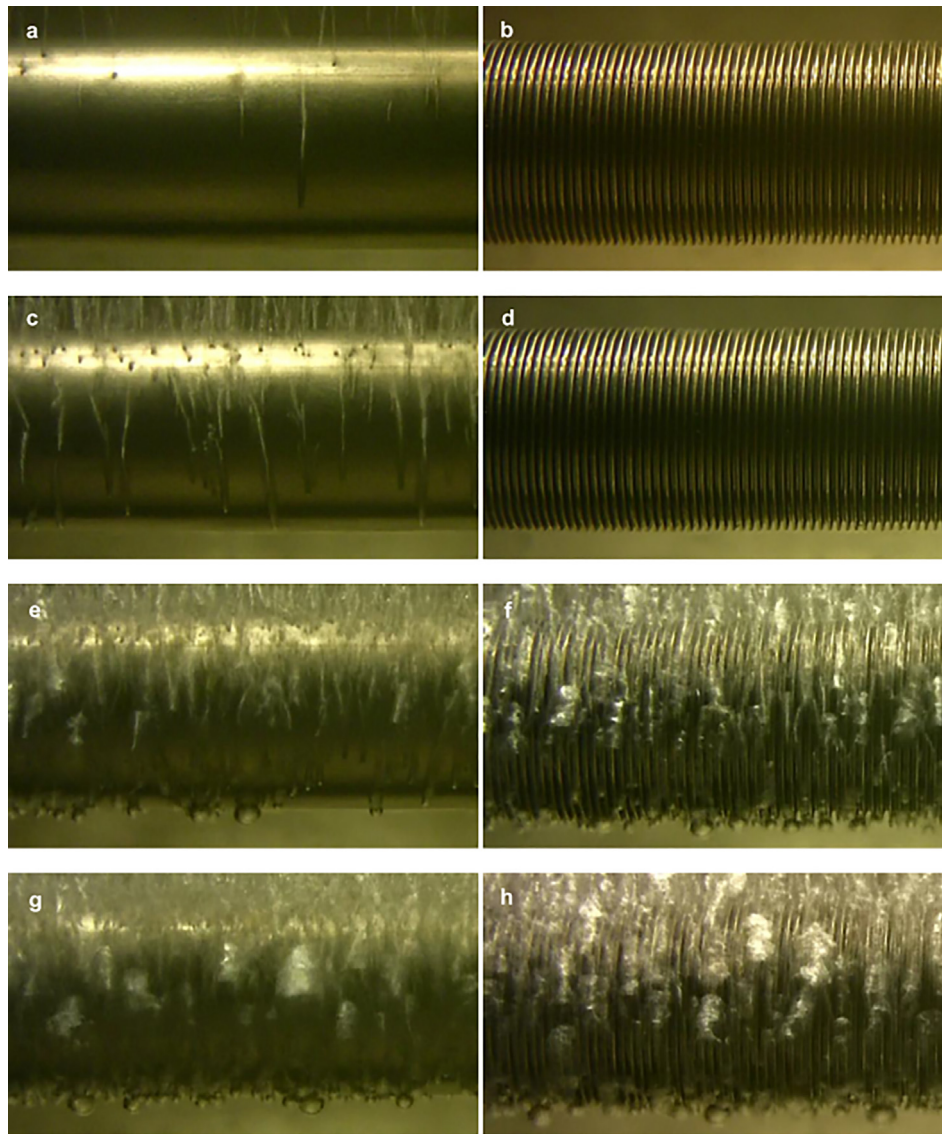


Fig. 15. Pool boiling process of NH_3 . (a) Plain tube and 3300 W/m^2 . (b) Integral-fin tube at 3700 W/m^2 . (c) Plain tube at 11000 W/m^2 . (d) Integral-fin tube at 10200 W/m^2 . (e) Plain tube at 29900 W/m^2 . (f) Integral-fin tube at 28400 W/m^2 . (g) Plain tube at 47900 W/m^2 . (h) Integral-fin tube at 50600 W/m^2 . (from Fernández-Seara et al. [93]).

Surprisingly, few studies focus on the pool boiling heat transfer of carbon dioxide [23], and only one of them investigates an enhanced surface. In 2016, Liu et al. [96] reported the pool boiling performance of CO_2 on a plain and three screwed (integral-fin) tubes with different structural parameters (E1, E2, E3). The experimental saturation pressure varied from 2 MPa to 4 MPa, and the heat fluxes varied from 10 kW/m^2 to 50 kW/m^2 . The performance of the three screwed tubes were better than the plain tube, and the HTC enhancement factors were in the ranges of 1.5–1.7, 1.6–1.8, and 2.0–2.2 for the tubes E1, E2, and E3, respectively. Liu et al. [96] also found that the enhancement factor decreased with increasing heat flux.

4. Predictive methods

This section chronologically describes the development of mechanistic based models and empirical correlations for the prediction of enhanced pool boiling. The governing equations for the predictive methods for the structured surfaces and for the porous surfaces are given in Tables 6 and 7, respectively.

4.1. Structured surfaces

Nakayama et al. [97] were one of the first to establish a mechanistic based model for pool boiling on structured enhanced surfaces. They developed the model based on their visual observations of boiling on the Thermoexcel-E tube, which has rectangular sub-surface tunnels covered with triangular pores (Fig. 2d). Nakayama et al. [97] modelled the bubble cycle as the bubble originates inside the tunnel and migrates to the outside of the tunnel. One complete bubble cycle is divided into three phases: (i) the pressure build-up phase; (ii) the pressure reduction phase; and (iii) the liquid-intake phase. The total heat flux from the surface was calculated from a sum of the latent heat flux due to the thin-film evaporation inside the tunnels and the sensible heat flux due to the external convection. The model assumes that the evaporating liquid film exists only in the corners of the tunnel, and that the rest of the tunnel is filled by vapor. This assumption, however, cannot account for the presence of alternating liquid and vapor zones inside the tunnel with a thin liquid film separating the vapor zone from the tunnel wall, which was observed by Nakayama et al. in another paper in the same year (1980) [98].

Table 6
Summary of the predictive methods for pool boiling heat transfer of structured surface.

| Authors/year | Recommended geometry/applicable refrigerants and operating range | Major equations |
|---------------------------------|---|---|
| <i>Mechanistic based models</i> | | |
| Nakayama et al. (1980) [97] | Thermoexcel-E and the structured surface having interconnected tunnels and pores/generalized model validated by R11 | $q = q_{lat} + q_{ex}$ $q_{lat} = \frac{(m_{l1} + m_{l2})i_{lv}}{(a_1 + a_2)A_{base}}$ $m_{l1} = V_{vm}(\rho_{v1} - \rho_{v0}) + N_{pore} \cdot \frac{\pi d_{pore}^3}{12} \cdot \rho_{vm1}$ $m_{l2} = \theta_2 k_1 C_{i2} \Delta T_{i2} / i_{lv}$ $\theta_1 = \frac{V_{vm} i_{lv}}{k_1 C_{i1}} \left\{ \frac{\rho_{vm1} (i_{lv} - R T_{v0})}{R T_{v0}^2} \ln \left(\frac{T_w - T_{v0}}{T_w - T_{v1}} \right) + \frac{\rho_{vm1}}{\Delta T_{i1}} \ln \left(\frac{T_{v1}}{V_{v1}} \right) \right\}$ $\theta_2 = \sqrt{\frac{\eta_d^3}{5.242} \left[0.1457 - 0.0329 C_0 \left(\frac{\rho_{vm2}}{\rho_l} \right) \eta_d^4 \right] \cdot \frac{\rho_l r_{pore}^3}{\sigma}} \cdot \eta_d = \frac{d_{bb}}{2r_{pore}} \left[1 + \sqrt{1 - \left(\frac{2r_{pore}}{d_{bb}} \right)^2} \right]$ $q_{ex} = \left(\frac{\Delta T_s}{C_q} \right)^{5/3} (N_{ap} / A_{base})^{1/3}$ $N_{ap} = \frac{\Phi \cdot \theta_2^2 - \zeta_3 (\zeta_2^2 + 3) + 4}{\eta_d (\eta_d^2 + 3) - 4} \cdot N_{pore}$ $\zeta_3 = -C_3 \left(\frac{m_{l1} + m_{l2}}{\rho_l N_{pore} \pi r_{pore}^2} \right)^{1/3}$ <p>C_{i1}, C_{i2}, C_3, C_q, C_0 and C_b are six empirical constants. note: the length unit in this model is [cm]</p> |
| Xin and Chao (1987) [100] | T-shape finned surface/generalized model validated by R11 and water | $Nu = C_1 \frac{2H_{fin} + W_{fin}}{W_{fin}} Ar^{1/3} Re^{C_2} We^{C_3} Pr^{C_4}$ $Ar = \frac{g W_{fin}^3}{\nu_l^2} \cdot \frac{\rho_l - \rho_v}{\rho_l}$ $We = \frac{q_{ex}^2 S_{fin}^2}{\sigma \rho_v i_{lv} W_{fin}}$ |
| Haider (1994) [35] | Structured surface having sub-surface tunnels/generalized model validated by R11, nitrogen, and water | $q = q_{tun} + q_{ex}$ $q_{tun} = \frac{\pi}{6} \rho_v i_{lv} d_{bb}^3 n_s$ $f = \frac{12 Q_{m1}}{\pi \rho_v i_{lv} d_{bb}^3}$ $Q_m = -2\pi r_{tun} k (T_w - T_{l,t}) \int_0^1 \frac{\zeta d\zeta}{\sqrt{\sec^2 \theta - \zeta^2} \ln \zeta}$ $d_{bb} = c_b \left[\frac{2\sigma}{(\rho_l - \rho_v) g} \right]^{1/2} \cdot c_b = (3s_{gap} \sin \theta)^{1/3} \left[\frac{2\sigma}{(\rho_l - \rho_v) g} \right]^{1/2}$ $n_s = \frac{1}{s_f s_{bb}}, s_f \text{ is the specified transverse pitch of the tunnels, or "fins."}$ $q_{ex} = q_{ex,MR} \left\{ \frac{Pr^{1/6}}{2.64\pi (c + \frac{Pr^{1/6}}{1.32\pi})} + \frac{0.66\pi (c + \frac{Pr^{1/6}}{1.32\pi})}{Pr^{1/6}} \right\}$ $q_{ex,MR} = 2\sqrt{\pi k_l \rho_l C_p f} d_{bb}^2 n_s \Delta T_s$ |
| Chien and Webb (1998) [101] | Tubular surfaces having sub-surface tunnels with surface pores/generalized model validated by R11, R123, R134a, and R22 | <p>This model predicts the total heat flux (q) for given wall superheat (ΔT_s) and dimensions (d_{pore}, p_{pore}, p_{fin}, H_{tun}) by the following procedure.</p> <ol style="list-style-type: none"> (1) Calculate the departure diameter (d_{bb}) by $d_{bb} = \left[\frac{Bo + \sqrt{Bo^2 + 2304(96/Bo - 3)}}{192 - 6Bo} \right]^{1/2} d_{pore} \text{ (Eq. A1)}$ (2) Calculate the bubble growth period (Δt_g) by $\Delta t_g = \frac{1}{C_{ig}} \left[\frac{7}{\pi} \cdot \frac{\rho_l T_s}{i_{lv} \rho_v \Delta T_s} \cdot \frac{d_{bb} - d_{pore}}{d_{bb} + d_{pore}} \right]^{1/2} \cdot \frac{d_{bb} - d_{pore}}{2}, C_{ig} = 0.0296 \text{ (Eq. A2)}$ (3) Calculate the initial liquid meniscus radius ($R_{m,i}$) by $R_{m,i} = \left[R_{m,e}^2 + \frac{\Delta A_{l,cyc}}{N_m (1 - \pi/4)} \right]^{0.5} \text{ (Eq. A3)}$ $\Delta A_{l,cyc} = \frac{4 - \pi}{2} \cdot 4.71 \times 10^{-9} \cdot \Delta T_s^{0.1882} d_{pore}^{0.609} (H_{tun} + W_{tun})^{1.49} \cdot \frac{\sigma^{0.512}}{\mu_l^{1.7712}} \text{ (Eq. A4)}$ (4) Calculate the latent heat transferred in the tunnels during the bubble cycle by integrating Eqs. (A5) with stepwise decreasing R_m from $R_{m,i}$ to $R_{m,e}$. $Q_{tun} = \int_0^{1/f} \left\{ 2\Delta T L_{tun} N_m \int_0^{\pi/4} \frac{k_l}{ R_m(t) + \delta_{me}(t) \sec(\phi) - R_m(t)} R_m(t) d\phi \right\} dt \text{ (Eq. A5)}$ (5) Calculate the waiting period (Δt_w) by Eqs. (A5 to A8), and find the meniscus radius $R_{m,g}$ at the beginning of the bubble growth period. $R_{m,t} = \left[R_{m,t-\Delta t}^2 + \frac{\Delta V_{l,\Delta t}}{L_{tun} N_m (1 - \pi/4)} \right]^{0.5} \text{ (Eq. A6)}$ $\Delta V_{l,\Delta t} = \Delta t \frac{2L_{tun} N_m \Delta T_s}{i_{lv} \rho_l} \int_0^{\pi/4} \frac{k_l}{ R_m(t) + \delta_{me}(t) \sec(\phi) - R_m(t)} R_m(t) d\phi \text{ (Eq. A7)}$ $\int_0^{\Delta t_w} \frac{dQ_{tun}}{\Delta T_s} dt = V_{vm} i_{lv} \left[\frac{\rho_v (i_{lv} - R T_{v0})}{R_g T_{v0}^2} \ln \left(\frac{T_w - T_{v0}}{T_w - T_{v1}} \right) + \frac{\rho_v}{\Delta T_{i1}} \ln \left(\frac{V_{v1}}{V_{v0}} \right) \right] \text{ (Eq. A8)}$ (6) Continue the calculation of the tunnel heat flux as for the bubble growth period, and calculate by decreasing R_m for $\Delta t_w < t < \Delta t_w + \Delta t_g$. (7) Sum the tunnel heat flux (q_{tun}) during Δt_w and Δt_g, and get the bubble frequency: $f = \frac{1}{\Delta t_w + \Delta t_g}$ (Eq. A9) (8) Calculate nucleation site density: $n_s = \frac{q_{tun}}{\rho_v i_{lv} f (\pi d_{bb}^2 / 6)} \text{ (Eq. A10)}$ (9) Calculate the external heat flux (q_{ex}) by $q_{ex} = 2\sqrt{\pi k_l \rho_l C_p f} \cdot d_{bb}^2 n_s \Delta T_s \cdot \sqrt{1 + \left(\frac{0.66\pi c}{Pr^{1/6}} \right)^2}, c = 6.42 \text{ (Eq. A11)}$ (10) Calculate the total heat flux $q = q_{ex} + q_{tun}$ <p>Procedure for predicting total heat flux: (1) Calculate the bubble departure diameter (d_{bb}) using $F_{dwy} + F_{st} + F_{bi} = F_B + F_L$</p> |
| Ramaswamy et al. (2003) [102] | Surfaces having orthogonal sub-surface tunnels with pores at intersection points/generalized model validated by FC72 | <p>Procedure for predicting total heat flux: (1) Calculate the bubble departure diameter (d_{bb}) using $F_{dwy} + F_{st} + F_{bi} = F_B + F_L$</p> |

Table 6 (continued)

| Authors/year | Recommended geometry/applicable refrigerants and operating range | Major equations |
|----------------------------|---|---|
| | | $F_{dwy} = \frac{3}{2} \rho_l \pi A^2 C_s R^2$ $F_{st} = \sigma \pi d_{pore} \sin \theta, \theta = \sin^{-1} \left(\frac{d_{pore}}{d_{bb}} \right)$ $F_B = (\rho_l - \rho_v) g V_{bb}, V_b = \frac{\pi}{3} \left[\frac{d_{bb}^3}{4} + \left(\frac{d_{bb}^2}{4} + \frac{d_{pore}^2}{8} \right) \sqrt{d_{bb}^2 - d_{pore}^2} \right]$ $F_L = 2\pi \rho_l (d_{bb} A')^2 C_L, C_L = 1.2$ $F_{bt} = A^2 \rho_v \frac{\pi}{3} \left\{ \frac{3}{4} d_{bb}^2 + \frac{1}{4} \cdot \frac{d_{bb}^3 - 2d_{bb}d_{pore}^2}{\sqrt{d_{bb}^2 - d_{pore}^2}} - \frac{2d_{bb}d_{pore}^2}{8\sqrt{d_{bb}^2 - d_{pore}^2}} \right\}$ <p>(2) Calculate the initial meniscus radius using</p> $r_{m,i} = \left[\frac{\Delta A_{yc}}{N_m(1-\frac{3}{4})} + \frac{\sigma}{\Delta T_s} \frac{T_{i0}}{\rho_{v0} h_{lv}} \right]^{\frac{1}{2}}$ <p>(3) Calculate the latent heat transfer inside the tunnel during the waiting period ($Q_{tun,w}$) and the waiting period (Δt_w) by</p> $\int_0^{\Delta t_w} \frac{dQ_{tun}}{dt} dt = i_{lv} [V_{vm}(\rho_{v1} - \rho_{v0}) + \rho_{vm}(V_{v1} - V_{v0})]$ <p>Small steps are chosen to solve the above equation until the right-hand side and left-hand side values matched within 5%. After every time step, a new meniscus radius ($r_{m,new}$) is calculated using</p> $r_{m,new} = \left[r_{m,old}^2 - \frac{\Delta V_l}{LN_m(1-\pi/4)} \right]^{1/2}, \Delta V_l = \Delta t \frac{2LN_m}{\rho_{lv}} \int_0^{\pi/4} \frac{k_l \Delta T_s}{ r_m(t) + \delta_{mc} \sec \phi - r_m(t)} r_m(t) d\phi$ <p>The meniscus radius at the end of the waiting period ($r_{m,g}$) becomes the initial value for the growth period.</p> <p>(4) Calculate the growth period (Δt_g) using</p> $\Delta t_g = \frac{1}{c_g} \left(\frac{7}{\pi} \cdot \frac{\rho_l \Delta T_s}{\rho_{lv} h_{lv}} \cdot \frac{d_{bb} + d_{pore}}{d_{bb} - d_{pore}} \right)^{1/2} \frac{d_{bb} - d_{pore}}{2}, c_g = 0.0296$ <p>(5) Calculate the latent heat transfer inside the tunnel during the growth period ($Q_{tun,g}$) similar to step 3.</p> <p>(6) Calculate the frequency of bubble departure (f) as $1/(\Delta t_w + \Delta t_g)$.</p> <p>(7) Calculate the total tunnel heat flux (q_{tun}) as $(Q_{tun,w} + Q_{tun,g})/A_{ex}$</p> <p>(8) Calculate the nucleation site density (n_s) using</p> $n_s = \frac{Q_{tun,w} + Q_{tun,g}}{\rho_{lv} i_{lv} f (\pi d_{bb}^2 / 6) A_{ex}}$ <p>(9) Calculate the external connective heat flux (q_{ex})</p> $q_{ex} = 2\sqrt{\pi k_l \rho_l C_p f} d_{bb}^2 n_s \Delta T_s \left[1 + \left(\frac{0.66\pi c}{Pr^{1/6}} \right)^{1/n} \right], c = 6.42$ <p>(10) Calculate the total heat flux as $q = q_{tun} + q_{ex}$</p> <p>Procedure for predicting total heat flux:</p> <p>(1) Calculate the bubble departure diameter (d_{bb}) using the force balance as given in Ramaswamy model (2003).</p> <p>(2) Calculate the initial film thickness by solve the following equations iteratively:</p> $\delta_0 = 1.3375 r_{tun} \left(\frac{\mu_{w0}}{\sigma} \right)^{2/3}$ $u_0 = \frac{4k_l \Delta T_s}{\rho_{lv} h_{lv} T_{tun}} \sqrt{\frac{r_{tun}}{\delta_0}} \tan^{-1} \sqrt{\frac{r_{tun}}{\delta_0}}$ <p>(3) Calculate the bubble departure frequency by solving</p> $q_{tun} = \int_0^{1/2f} (2q_{menisci} + q_{film})_{exp} dt + \int_{1/2f}^1 (2q_{menisci} + q_{film})_{con} dt = \frac{\pi}{6} \rho_v i_{lv} d_{bb}^3$ <p>(4) Calculate the nucleation site density by</p> $n_s = C(\Delta T)^{a_1} N_s^{a_2} r_{tun}^{a_3} d_{pore}^{a_4}$ $C = 1246.38, a_1 = 0.912, a_2 = 0.435, a_3 = 0.762, a_4 = -0.545$ <p>(5) Calculate the total heat flux by</p> $q = n_s q_{tun} + q_{ex}$ $q_{ex} = 2\sqrt{\pi k_l \rho_l C_p f} d_{bb}^2 n_s \Delta T_s \left[1 + \left(\frac{0.66\pi c}{Pr^{1/6}} \right)^{1/n} \right]$ $c = b_0 + b_1 \Delta T_s + b_2 \Delta T_s^2 + b_3 \Delta T_s^3, b_0 = 6.58, b_1 = -1.1612, b_2 = 0.0782, b_3 = 0.0018$ $q = q_{tun} + q_{ex}$ $q_{tun} = \frac{(m_1 + m_2) h_{lv} \beta}{(t_w + t_g + t_{in}) A}$ $m_{t1} = V_{im}(\rho_{v1} - \rho_v) + N \frac{\pi d_{pore}^2}{12} \rho_{vm1}$ $m_{t2} = (t_g + t'_{in} + t''_{in}) \frac{k_l [T_w - (T_{p1} + T_{p2})/2]}{h_{lv}} C_{t2}, C_{t2} = 2.773 \times 10^4 \text{ cm}$ $\beta = \frac{\rho^* t_g - \zeta (\zeta^3 + 3) + 4}{\eta_d (\eta_d^3 + 3) - 4}$ $\rho^* = \frac{6k_l C_{t2} \Delta T_{t2}}{\rho_{vm2} h_{lv} \sqrt{2\sigma/d_{pore}} \rho_l N \pi d_{pore}^2 / 4}$ $t_g^* = t_g / \sqrt{\frac{\rho_l d_{pore}^2}{8\sigma}}$ $\zeta = -C_3 \left[\frac{8(m_1 + m_2)}{\rho_l N \pi d_{pore}^2} \right]^{1/3}$ $\eta_d = \frac{d_{bb}}{d_{pore}} \left[1 + \sqrt{1 - \left(\frac{d_{pore}}{d_{bb}} \right)^2} \right]$ $t_w = \left(\frac{t_g Q}{2P'} - \frac{P'}{2Q} \right)^2$ $P' = \frac{d_{bb}}{4J \sqrt{3\pi}} - \sqrt{t_g}, Q = \frac{T_{inf} - T_w}{T_w - T_s}$ $t_g = 33.784 \left(\frac{7}{\pi} \cdot \frac{\rho_l \Delta T_s}{\rho_{lv} h_{lv}} \cdot \frac{d_{bb} + d_{pore}}{d_{bb} - d_{pore}} \right)^{1/2} \frac{d_{bb} - d_{pore}}{2}$ |
| Murthy et al. (2006) [103] | Surfaces having tunnels and pores (especially the tunnels with circular cross-section)/generalized model validated by R123, FC72, and R11 | |
| Das et al. (2007) [104] | Surfaces having tunnels and pores/generalized model validated by R11 | |

Table 6 (continued)

| Authors/year | Recommended geometry/applicable refrigerants and operating range | Major equations |
|-----------------------------------|--|---|
| Pastuszko et al. (2008) [105] | Surfaces having connected horizontal and vertical tunnels/generalized model validated by R123 | $t_{in} = \frac{\pi d_{bb}^3 \rho_{v2}}{3 d_{pore}^2 C_v \sqrt{2gH_l}}$ $q_{ex} = q_{ex,MR} \left\{ 1 + \frac{0.66\pi c}{Pr^{1/6}} \right\}, \quad c = 6.42$ $q_{ex,MR} = 2 \sqrt{\pi k_l \rho_l C_p f d_{bb}^2 n_s \Delta T_s}, \quad n_s = \frac{q_{tun}}{\rho_v i_{lv} \pi d_{bb}^2 / 12}$ $q = (q_H + q_V) / 2$ <p>- q_H and q_V are the heat fluxes in horizontal and vertical tunnels, respectively.</p> $q_H = q_{tun,H} n_s H P_{pore} W_{tun} + q_{ex,H}$ $q_{tun,H} = \frac{\dot{Q}_{0-2,H}}{2 P_{pore} (W_{tun} + H_{tun})}$ $\dot{Q}_{0-2,H} = 8 k_l \Delta T_s P_{pore} \ln \frac{\rho_{v,0-2,H} + \sqrt{2} \delta_{ne}}{\sqrt{2} \delta_{ne}}$ $\delta_{t,0-2,H} = \sqrt{\frac{V_{10,H} + V_{12,H}}{8 P_{pore}}}$ $V_{10,H} = \frac{\rho_{v2} \left(V_{tun,H} + \frac{\pi d_{bb}^3}{6} \right) - (\rho_l - \rho_{v2}) \Delta V_{1,0-2,H} - \rho_{v2} V_{tun,H}}{\rho_{v2} - \rho_{v1}}$ $d_{bb,H} = \left(\frac{Bo + \sqrt{Bo^2 + 2304(96/Bo - 3)}}{192 - 6Bo} \right)^{1/2} d_{pore}$ $V_{12,H} = V_{10,H} - \Delta V_{1,0-2,H}, \quad \Delta V_{1,0-2,H} = \frac{2V_{tun,H} + (\pi d_{bb}^3)/6}{2} \frac{\rho_{v2} - \rho_{v1}}{\rho_l} + \frac{\pi d_{bb}^3}{6} \frac{\rho_{v2} + \rho_{v1}}{2\rho_l}$ $\delta_{ne} = \left(\frac{\Delta T_s}{\rho_l i_{lv} \Delta T_s} \right)^{1/3}$ $n_s H = \frac{q_{tun,H}}{\rho_{tun} i_{lv} f \frac{\pi d_{bb}^3}{6}}$ $f_H = \frac{1}{\Delta t_{0-1,H} + \Delta t_{1-2,H}}$ $\Delta t_{0-1,H} = \frac{i_{lv} \rho_l \Delta V_{1,0-1,H}}{Q_{0-1,H}}$ $\Delta t_{1-2,H} = \frac{1}{C_{ig}} \left[\frac{7}{\pi} \cdot \frac{\rho_l T_s}{i_{lv} \rho_{v1} \Delta T_s} \cdot \frac{d_{bb,H} - d_{pore}}{d_{bb,H} + d_{pore}} \right]^{1/2} \cdot \frac{d_{bb} - d_{pore}}{2}, \quad C_{ig} = 0.0296$ $q_{ex,H} = 2 \sqrt{\pi k_l \rho_l C_p f_H d_{bb}^2 n_s H \Delta T_s}$ $q_V = q_{tun,V} \frac{W_{tun}}{P_{tun}} + q_{ex,V}$ $q_{tun,V} = \frac{\dot{Q}_{0-2,V}}{2 H_{fin} (W_{tun} + H_{tun})}$ $q_{ex,V} = 2 \sqrt{\pi k_l \rho_l C_p f_V d_{bb}^2 n_s V \Delta T_s} P_{tip} P_{tip}^c$ $q = q_{tun} + q_{ex}$ $q_{tun} = \rho_v i_{lv} n_s \frac{\pi d_{bb}^3}{6} f$ $n_s = \frac{1}{P_{tun} (\delta_{fin} + \delta_{fin})}$ $d_{bb} = \left\{ 6\sigma \frac{2W_{tun} \delta_{fin}}{W_{tun} + \delta_{fin}} / [g(\rho_l - \rho_v)] \right\}^{1/3}$ $f = \frac{1}{\Delta t_{0-1} + \Delta t_{1-2} + \Delta t_{2-3}}$ $\Delta t_{0-1} = 0.19 \frac{W_{tun}}{J_a}$ $\Delta t_{1-2} = \frac{1}{C_{ig}} \left[\frac{7}{\pi} \cdot \frac{\rho_l T_s}{i_{lv} \rho_{v1} \Delta T_s} \cdot \frac{d_{bb} - W_{tun}}{d_{bb} + W_{tun}} \right]^{1/2} \cdot \frac{d_{bb} - W_{tun}}{2}, \quad C_{ig} = 0.06$ $\Delta t_{2-3} = \frac{2\rho_l d_{bb}^2}{3\rho_l d_{pore}^2 v_l \delta_{fin} / P_{pore}}$ $q_{ex} = n q_m \cdot 2(2H_{fin} + d_{bb} + \pi d_{bb}) d_{bb}$ $q_m = 2 \sqrt{\frac{k_m C_{p1} \rho_l f}{\pi} \cdot \frac{\Delta T}{\cosh[m_{fin} (H_{fin} + \delta_{fin}/3)]}} m_{fin} = \sqrt{\frac{2(\delta_{fin} + P_{tun} - W_{tun}) q_{tun} / \Delta T}{k_{Cu} \delta_{fin} (P_{tun} - W_{tun})}}$ |
| Pastuszko (2012) [106] | Surfaces having connected horizontal and vertical tunnels/water for 100–600 kW/m ² , ethanol for 50–150 kW/m ² , and R123 for 30–300 kW/m ² | $q = q_{tun} + q_{ex}$ $q_{tun} = \rho_v i_{lv} n_s \frac{\pi d_{bb}^3}{6} f$ $n_s = \frac{1}{P_{tun} (\delta_{fin} + \delta_{fin})}$ $d_{bb} = \left\{ 6\sigma \frac{2W_{tun} \delta_{fin}}{W_{tun} + \delta_{fin}} / [g(\rho_l - \rho_v)] \right\}^{1/3}$ $f = \frac{1}{\Delta t_{0-1} + \Delta t_{1-2} + \Delta t_{2-3}}$ $\Delta t_{0-1} = 0.19 \frac{W_{tun}}{J_a}$ $\Delta t_{1-2} = \frac{1}{C_{ig}} \left[\frac{7}{\pi} \cdot \frac{\rho_l T_s}{i_{lv} \rho_{v1} \Delta T_s} \cdot \frac{d_{bb} - W_{tun}}{d_{bb} + W_{tun}} \right]^{1/2} \cdot \frac{d_{bb} - W_{tun}}{2}, \quad C_{ig} = 0.06$ $\Delta t_{2-3} = \frac{2\rho_l d_{bb}^2}{3\rho_l d_{pore}^2 v_l \delta_{fin} / P_{pore}}$ $q_{ex} = n q_m \cdot 2(2H_{fin} + d_{bb} + \pi d_{bb}) d_{bb}$ $q_m = 2 \sqrt{\frac{k_m C_{p1} \rho_l f}{\pi} \cdot \frac{\Delta T}{\cosh[m_{fin} (H_{fin} + \delta_{fin}/3)]}} m_{fin} = \sqrt{\frac{2(\delta_{fin} + P_{tun} - W_{tun}) q_{tun} / \Delta T}{k_{Cu} \delta_{fin} (P_{tun} - W_{tun})}}$ |
| Pastuszko and Wójcik (2015) [108] | Surfaces having sub-surface tunnels covered with surface pores/water for 30–760 kW/m ² , FC72 for 6–50 kW/m ² | $q = q_{tun} + q_{ex}$ $q_{tun} = \rho_v i_{lv} n_s m \frac{\pi d_{bb}^3}{6} f$ $n_{s,m} = \frac{4(\delta_{fin} P_{tun} + \delta_{fin} W_{tun})}{\pi d_{bb}^2} \frac{1}{P_{tun} (\delta_{fin} + \delta_{fin})}$ $d_{bb} = \left[\frac{6\sigma d_{pore}}{g(\rho_l - \rho_v)} \right]^{1/3}$ $f = \frac{1}{\Delta t_{0-1} + \Delta t_{1-2}}$ $\Delta t_{0-1} = 3\Delta t_{1-2}$ $\Delta t_{1-2} = \frac{1}{C_{1-2}} \left[\frac{7}{\pi} \cdot \frac{\rho_l T_s}{i_{lv} \rho_{v1} \Delta T_s} \cdot \frac{d_{bb} - W_{tun}}{d_{bb} + W_{tun}} \right]^{1/2} \cdot \frac{d_{bb} - W_{tun}}{2}, \quad C_{1-2} \text{ is empirical constant}$ $q_{ex} = 2 \sqrt{\pi k_l \rho_l C_p f d_{bb}^2 n_{s,m} \Delta T_s} P_{tip}$ $\Delta T_{s,tip} = \frac{\Delta T_s}{\cosh[m(H_{fin} + \delta_{fin}/2)]}$ $m = \sqrt{\frac{2\alpha_m (\delta_{fin} + P_{tun} - W_{tun})}{k_{Cu} \delta_{fin} (P_{tun} - W_{tun})}}, \quad \alpha_m = \frac{q_{tun}}{\Delta T_s}$ |
| Kedzierski et al. [72] | Turbo-ESP surface/R134a and R1234yf (for pure), R513A and R450A (for mixture), for 20–110 kW/m ² | <p>For pure:</p> $q'' = 42 \times 10^4 \times i_{lv} \rho_v \left(\frac{\sigma}{\rho_l - \rho_v} \right)^{3/2} \Delta T_s^{7.51} \sqrt{\frac{\mu \sigma}{c_{p1} (\rho_l - \rho_v)}};$ <p>For mixture:</p> $q'' = 42 \times 10^4 \times i_{lv} \rho_v \left(\frac{\sigma}{\rho_l - \rho_v} \right)^{3/2} \cdot T_s^{7.51} \sqrt{\frac{\mu \sigma}{c_{p1} (\rho_l - \rho_v)}} \left(1 - \frac{1.29 \Delta T_s}{7.51 \sqrt{\frac{\mu \sigma}{c_{p1} (\rho_l - \rho_v)}}} \right)$ |

Table 6 (continued)

| Authors/year | Recommended geometry/applicable refrigerants and operating range | Major equations |
|-----------------------------------|--|--|
| Correlations | | |
| Rainey et al. (2003) [110] | Square pin-finned surface/FC72 for approximately 50–1200 kW/m ² | For low heat flux: $q = 5.49 \times 10^4 \cdot \Delta T_s - 8.68 \times 10^6 \cdot P^{-0.814}$ for high heat flux: $q = (284P + 1670\Delta T_{\text{subcooling}} + 84200)\Delta T_s^{0.6}$ |
| Wen and Ho (2003) [111] | Surface with V-shaped cavities/water for 0.3–51 kW/m ² | $\frac{C_{p,l}\Delta T_s}{h_{lv}} = C_{sf} \left[\frac{q}{\mu_{lv}} \sqrt{\frac{g\sigma}{g(\rho_l - \rho_v)}} \left(1 + \sin \frac{\theta_{\text{cavity}}}{2}\right) \right]^{0.33} Pr^s$ θ_{cavity} is the angular spacing of the V-shaped cavity. s equals to 1 for water and 1.7 for all other fluids. |
| Rajulu (2004) [112] | Reentrant cavity surface/acetone, isopropanol, ethanol, and water, for 11–42 kW/m ² | HTC enhancement: $E_{HTC} = aq^b x_{\text{mouth}}^c$ a , b , c are experimentally determined constants, x_{mouth} is the size of reentrant cavity mouth |
| Christians and Thome (2012) [113] | Enhanced tube with reentrant channels (Turbo-Bii, Gewa-B, High Flux, Turbo-EDE2, Gewa-B4, Turbo-B5, Gewa-B5, 3D)/R134a and R236fa, for 20–80 kW/m ² | $h_{pb} = 41.6 \times 10^3 \cdot \left(\frac{q^2}{h_{lv} Pr^2}\right)^{-0.13} \cdot G_{t-s}^{1.66} \cdot \frac{k_f}{D}$ For Turbo-Bii enhanced tube: $G_{t-s} = 0.118$ For Gewa-B enhanced tube: $G_{t-s} = 0.1141$ For High Flux enhanced tube: $G_{t-s} = 0.2024$ For Turbo-EDE2 enhanced tube: $G_{t-s} = 0.1488$ For Gewa-B4 enhanced tube: $G_{t-s} = 0.1777$ For Turbo-B5 enhanced tube: $G_{t-s} = 0.1584$ For Gewa-B5 enhanced tube: $G_{t-s} = 0.1597$ For 3D enhanced tube: $G_{t-s} = 0.1486$ |
| van Rooyen and Thome (2013) [67] | Enhanced tube with reentrant channels (Turbo-B5, Gewa-B5)/R134a, R236fa and R-1234ze, for 15–70 kW/m ² | $h_{pb} = a \left\{ \left(\frac{A_H}{\Delta T_s}\right)^{1/3} \left(\frac{\rho_l h_{lv}}{k_f \mu_{lv}}\right)^{2/3} \right\}^b \cdot \frac{k_f}{D} \left[1 - \frac{1}{(\Delta T_s + 1)^{1/2}}\right]$ For Turbo-B5 enhanced tube: $a = 2711$, $b = 0.48$ For Gewa-B5 enhanced tube: $a = 967$, $b = 1.06$ |
| Ho et al. (2016) [114] | Surface having intrinsic micro-cavities and/or micro-fins/FC72 for approximately 6–36 kW/m ² | $q = \mu_{lv} \left[\frac{g(\rho_l - \rho_v)}{\sigma} \right]^{1/2} \left[\frac{C_{p,l}\Delta T_s}{C_{g,hv} Pr^{1.5}} \right]$ $C_{sf} = 3.21 \times 10^{-5} \cdot F_{sr}^{0.0469}$ $n = 1.2163 F_{sr}^{-0.0743}$ F_{sr} is surface roughness factor, which equals to the ratio of actual solid area to projected area. |

In a later paper, Nakayama et al. [99] identified three possible evaporation modes for structured surfaces that have sub-surface tunnels and surface pores: dried-up mode, suction-evaporation mode, and flooded mode, as schematically shown in Fig. 16. In the dried-up mode, bubbles are generated at the surface pores outside the sub-surface tunnels that are filled with vapor. Because all the pores serve as nucleation sites, the heat transfer mechanism for the dried-up mode is analogous to that of nucleate boiling on a plain surface. In the suction-evaporation mode, some of the surface pores are active while others are inactive. Bubbles are generated at active pores, which produces a pumping action that sucks the bulk liquid into the tunnel space through inactive pores. Nakayama et al. [99] stated that the “suction-evaporation mode” yields the highest heat transfer performance due to evaporation of liquid on the tunnel walls. In the flooded mode, most of the tunnel space is occupied by liquid, and bubbles are generated at the few active pores that operate like isolated nucleation sites. With the increase of heat flux, the evaporation could transition from the flooded mode to the suction-evaporation mode, and then to the dried-up mode. However, Nakayama et al. [99] did not provide a criterion to define the relationship between the three evaporation modes and heat flux. From the viewpoint of the evaporation modes, the Nakayama et al. [97] model only accounts for the suction-evaporation mode.

Xin and Chao [100] proposed a countercurrent two-phase boiling model for T-shaped finned surfaces. According to their observation, the vapor bubbles coalesce at the narrow opening and stream out from the channel at a threshold pressure. They considered this phenomenon as countercurrent two-phase flow, i.e., the vapor flows upwards and out of the tunnel while the liquid simultaneously flows downwards into the tunnel along the wall. The model assumes that the flow is steady instead of cyclic, and it does not incorporate the periodic bubble growth and departure, the bubble size, or the bubble frequency. In addition, the model does not con-

sider the nucleation site density because the entire between-fin regions are assumed to be active. Because the model did not account for the periodic nature of bubble evolution, which typically exists over a broad range of heat fluxes, Haider [35] argued that the Xin and Chao [100] model was based on physically unrealistic assumptions.

Apparently dissatisfied with the Xin and Chao [100] model, Haider [35] constructed his own pool boiling heat transfer model, which was a function of the fluid properties and the structured surface geometry. Haider [35] modelled boiling surfaces with two-dimensional slot openings, or pores on the top surface, with a variety of tunnel cross-section shapes. The model is based on the boiling mechanism of “flooded mode,” which assumes alternate zones of liquid slugs and vapor plugs in the sub-surface tunnels. It’s noted that this model uses only one empirical constant. Haider [35] also proposed a criterion for the boiling mode transition from the “flooded mode” to the “suction-evaporation mode.” He stated that increasing wall superheat leads to higher bubble frequency with a smaller liquid slug to satisfy the momentum requirement. As the liquid slugs inside the tunnel becomes larger, they coalesce when two menisci meet. The transition from flooded to suction-evaporation occurs when both the menisci touch each other.

Chien and Webb [101] improved the Nakayama et al. [97] model and reduced the number of empirical constants from six to two. Though both of the models are based on the “suction-evaporation mode”, the Chien and Webb [101] model accounts for the temporal evaporation rate variation inside tunnels as well as the dynamic nature of the convection heat transfer outside of the tunnels by analyzing the meniscus thickness, the bubble departure diameter, and the bubble growth, which are neglected in the Nakayama et al. [97] model. The Chien and Webb [101] model is applicable to tubular surfaces having sub-surface tunnels with surface pores, for arbitrary combinations of the pore diameter, the pore pitch, the fin pitch, and the tunnel height.

Table 7
Summary of the predictive methods for pool boiling heat transfer of porous surface.

| Authors/year | Recommended geometry/applicable refrigerants and operating range | Models/correlation |
|-------------------------------------|--|---|
| O'Neill et al. (1972) [115] | Surface coated by sintered particles/not provided | $\Delta T_s = \frac{\beta q r_{bb}^2}{k_l} + \frac{2\sigma}{(\frac{d\mu}{dP})_{r_{bb}}} r_{bb}$ $\beta = \frac{1}{\delta_c} \left[1 - (1 - \epsilon) \left(1 + \frac{V_{ph}}{\delta_c A_{p,base}} \right) \right] \left(\frac{\delta_c A_{p,base}}{A_p r_{bb}} \right)^2$ |
| Conwell et al. (1976) [116] | Surface covered by a thin porous media/water for 100–600 kW/m ² | $q = C i_{lv} \left(\frac{A_p}{A} \right) \left(\frac{\Delta P \epsilon}{\delta} \right)^{1/(2+m)}$ |
| Ito and Nishikawa (1978) [117] | Surface coated by sintered particles/not provided | “Friction model”: $q = \sqrt{\frac{4\epsilon^3 d_{pore} \rho_l^2 \beta_{lv} \ln \frac{T_w}{T_s}}{7(1-\epsilon)\delta_c}}$ “Conduction model”: $q = [\epsilon k_l + (1 - \epsilon) k_p] \frac{\Delta T_s}{\delta_c}$ |
| Nishikawa and Ito (1982) [118] | Surface coated by sintered particles/not provided | $\frac{q \delta_c}{k_m \Delta T_s} = 0.001 \left(\frac{\sigma^2 i_{lv}}{q^2 \delta_c^2} \right)^{0.0284} \left(\frac{\delta}{d_p} \right)^{0.56} \left(\frac{q d_p}{\epsilon i_{lv} \mu_v} \right)^{0.593} \left(\frac{k_p}{k_m} \right)^{0.708} \left(\frac{\rho_l}{\rho_v} \right)^{1.67}$ $k_m = k_l + (1 - \epsilon) k_p$ |
| Zhai et al. (1982) [119] | Surface coated by sintered particles/not provided | $q = q_{boiling} + q_{conduction}$ $q_{boiling} = C i_{lv} v_0 \left(\frac{P_l + 2\sigma/r}{RT_s} \right)$ $q_{conduction} = \left(1 - \frac{A_p}{A} \right) [(1 - \epsilon) k_p + \epsilon k_l] \cdot \frac{\Delta T_s}{\delta_c}$ |
| Zhai et al. (1987) [120] | Surface coated by sintered particles/R11, R12, R22, R113 and R114, not provided with the operating range | $\frac{q \delta_c}{k_l \Delta T_s} = 0.49 \left(\frac{\rho_l}{\rho_v} \right)^{0.476} \left(\frac{\Delta T_s}{T_s} \right)^{0.485} \left(\frac{\delta}{d_p} \right)^{0.845} \left(\frac{\rho_p i_{lv}}{\rho_s} \right)^{-5.027}$ $\cdot \left(\frac{\Delta T_s \epsilon k_l}{\mu_v i_{lv}} \right)^{-0.588} \left[\frac{(1-\epsilon) k_p}{\epsilon k_l} \right]^{0.137} \left(\frac{d_{pore} \rho_v \sigma}{\mu_v^2} \right)^{1.432} \left(\frac{d_p P_l}{\sigma} \right)^{-0.432}$ |
| Kovalyov and Soloviyov (1990) [121] | Porous surface/generalized model validated by water and R22 | $k_l \frac{d^2 T}{dx^2} = h_v (T_{matrix} - T_l)$ $\frac{d^2 T_m}{dx^2} \left[\frac{2\sigma}{r_m} - G^2 f(r_m) \left(\frac{1}{\rho_l \epsilon_l^3} + \frac{1}{\rho_v \epsilon_v^3} \right) \right] = G \frac{dG}{dx} \left(\frac{1}{\rho_v \epsilon_v^3} - \frac{1}{\rho_l \epsilon_l^3} \right) + \frac{v_l G}{K_l} + \frac{v_v G}{K_v} + \frac{2f_l G^2}{\rho_v \epsilon_v^2}$ $P_v(x) - P_l(x) = \frac{2\sigma}{r_m(x)}$ $\frac{dP}{dx} = \frac{G v_l}{K_l}$ |
| Polyaev and Kichatov (2000) [122] | Porous coating/generalized model validated by water and R134a | For low ΔT_s : $q = C_1 \frac{i_{lv} \beta_{per} \rho_l^2 \delta_c}{\mu_v \sigma^2 T_s^3 (\rho_l - \rho_v) \epsilon} \Delta T_s^3$ for high ΔT_s : $q = C_2 \frac{\beta_{per} \rho_l (\rho_v i_{lv})^2}{\mu_v \delta_c T_s (\rho_l - \rho_v)} \Delta T_s$ C_1 and C_2 are empirical constants, β_{per} is the coefficient of absolute phase permeability $q = 3.71 \times 10^4 \cdot \Delta T_s - 3.22 \times 10^7 \cdot P^{-1.32}$ |
| Rainey et al. (2003) [123] | Porous-coated surface/FC72 for approximately 50–300 kW/m ² | |
| Zhang et al. (2012) [124] | Sponge-like nanoporous coated surface/generalized model validated by water | $q = \frac{\pi d_{bb}^2}{6} n_s f_{lv} \rho_v + \left(\frac{\Delta T_s}{b} \right)^a n_s^a + \frac{c k_l \delta_{lim} \Delta T_s}{1 - \cos \theta} n_s^a$ $a, b \text{ and } c \text{ are empirical constants; the other parameters are calculated using the equations in Nakayama et al. model}$ |

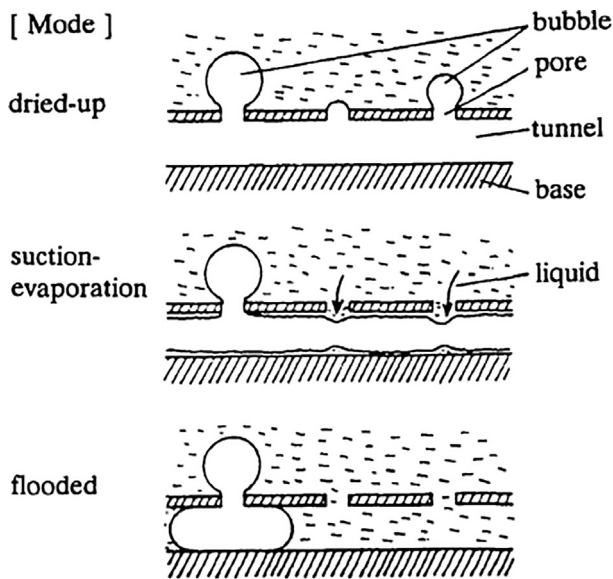


Fig. 16. Evaporation modes for structured surfaces with sub-surface tunnels and surface pores [99].

Ramaswamy et al. [102] developed a semi-analytical model to predict the bubble departure diameter, the frequency, and the nucleation site density for surfaces having orthogonal sub-surface tunnels with pores at intersection points. They adopted the “suction–evaporation mode” framework similar to Nakayama

et al. [97] and Chien and Webb [101]. Major improvements were made in the calculation for the bubble departure diameter, the evaporation within tunnels and the convective heat transfer from the external surfaces. They noted that the value of the Hamaker constant has a significant influence on the model prediction, and thus it needs to be accurately evaluated.

Murthy et al. [103] stated that the previous “suction–evaporation mode” based models (i.e., the models of [97,101,102]) failed to predict the observed bubble dynamics and the heat transfer performance on the structured surfaces with circular tunnels. They proposed a semi-analytical model based on the “flooded mode” assumption, and validated the model for data covering a range of dimensions for tunnel and pore. The model incorporates the dynamic forces in the calculation of the bubble departure diameter. Additionally, a correlation for the nucleation site density was developed based on the wall superheat and the geometry of the boiling structure.

Das et al. [104] found that the liquid refill stage was ignored in all previous studies. Based on the “suction–evaporation mode” assumption and the models of Nakayama et al. [97] and Chien and Webb [101], they developed a model for predicting the heat transfer and the bubble dynamics for surfaces with tunnels and pores. The Das et al. [104] model suggested that the liquid refill time was small compared to the duration of the suction–evaporation and flooded modes at large pool heights; however, the liquid refill time could be significant for smaller pool heights and for depressurized systems.

Pastuszko et al. [105] focused on the boiling heat transfer of “double-extended” surfaces that consist of connected horizontal

and vertical tunnels. They integrated the previous models of Nakayama et al. [97], Chien and Webb [101], and Ramaswamy et al. [102], with some modifications and simplifications. They developed a new analytical calculation for evaporating liquid volumes in the waiting and the growth periods, for the initial and the final vapor volume in the tunnel, and for the liquid volumes in the menisci for the beginning of the waiting period and the end of the growth period. According to their conclusions, the vertical tunnels have a more significant influence on the boiling heat transfer performance. Later, Pastuszko [106] modified his previous model [105] which refers to the joint area of the vertical tunnel and adjacent horizontal tunnels. They changed the calculation for waiting and growth periods, and added the calculation of liquid intake period. To incorporate the structure geometry, they modified the classical Mikic and Rohsenow correlation [107] by redefining the area of influence.

Pastuszko and Wójcik [108] proposed a simplified model based on their previous models [105,106] and the existing studies [97,101,102] for a micro-fin surface with sintered perforated foil, similar to the surfaces having sub-surface tunnels covered with surface pores. The Pastuszko and Wójcik [108] model requires only one empirical constant.

More recently, Kedzierski et al. [72] developed a model to predict both single-component and multi-component pool boiling of low-GWP refrigerants on the Turbo-ESP surface. The model accounts for viscosity effects on the bubble population and uses the Fritz equation [109] to account for increased vapor production with increasing superheat. Both loss of available superheat and mass transfer resistance effects were modeled for the refrigerant mixtures. For most heat fluxes, the model predicted the measured superheat to within ± 0.31 K. Both models are given in Table 6.

Besides the mechanistic based models discussed above, there are many correlations developed for pool boiling of structured surfaces. Rainey et al. [110] presented a simple $q - \Delta T$ correlation for square pin-finned surface using their FC-72 pool boiling data. Wen and Ho [111] proposed a correlation for pool boiling heat transfer in vertical/horizontal V-shaped geometries. Rajulu et al. [112] correlated the HTC enhancement of reentrant cavity tubes with heat flux, cavity mouth size, and three empirical constants. Christians and Thome [113] proposed a correlation for HTC as a function of heat flux, fluid properties, saturation pressure, tube diameter, and geometry factor. Their correlation is based on the pool boiling data of R-134a and R-236fa on seven commercial enhanced tubes (Turbo-Bii, Gewa-B, High Flux, Turbo-EDE2, Gewa-B4, Turbo-B5, and Gewa-B5). van Rooyen and Thome [67] developed a correlation based on boiling mechanisms in the near-wall region. This correlation incorporates the fluid properties, tube diameter, and two surface structure related parameters. The database for this correlation includes three refrigerants (R-134a, R-236fa and R-1234ze(E)) and two commercial enhanced tubes (Turbo-B5 and Gewa-B5). Ho et al. [114] developed a Rohsenow-model based correlation for the surfaces having intrinsic micro-cavities and/or micro-fins. The micro-features are reflected by a surface roughness in this correlation. Unfortunately, most of the existing correlations are not based on the databases that include low-GWP refrigerants, and their applicability for low-GWP refrigerants are not yet assessed, which could be carried out in the future studies. If poor predicting capabilities are found, the forms of these correlations could be still used as reference for new correlation development of low-GWP refrigerants.

4.2. Porous surfaces

The boiling models for the structured surface are not directly applicable to the porous surface due to the randomness of the porous surface geometry. Because of the irregular geometry, it is more

difficult to develop a mechanistic based model for the boiling heat transfer on porous surface. Consequently, few studies predicting the heat transfer on porous surfaces were found in the open literature.

O'Neill et al. [115] described an analytical model for pool boiling on a porous surface with the coating made of sintered particles. The assumptions, the deviation, and the limitations of the model were discussed in detail by Webb [33]. The key assumptions are: (i) the coating particles are spherical and of uniform diameter; (ii) the pores are uniform in size; (iii) each pore is active and thereby acts as a stable vapor trap. Webb [33] argued that such a static model cannot be justified because it assumes that a stable liquid film surrounds the bubble. However, this model presents several important fundamental concepts and serves as the starting point for developing a more complicated dynamic model.

Conwell et al. [116] developed a correlation for a surface covered by thin porous media based on their observations and experimental data. The main parameters of the correlation include the vapor covered surface area, the total surface area, the wick (coating) thickness, and the vapor pressure difference. As discussed by the authors, the main shortcoming of the model is the difficulty in obtaining a precise value for the vapor pressure difference.

Ito and Nishikawa [117] proposed two "critical models", i.e., the "friction model" and the "conduction model." The "friction model" assumes that vaporization occurs in the porous layer, and that the friction acting on the vapor when it escapes from the layer plays a significant role in boiling heat transfer. The "conduction model" assumes that the porous layer is filled with liquid and regards the porous layer as a uniform "thin layer." Based on this assumption, the heat flux is calculated as the thermal conduction through this "thin layer." Ito and Nishikawa [118] also developed a correlation based on their pool boiling data of R-11, R-113, and benzene on the surfaces coated by copper or bronze particles. The correlation incorporates the effects of porosity and thickness of the coating layer, particle diameter, and fluid properties.

Zhai [119] presented a modified model based on the previous studies [115–117]. The model calculates the heat flux by summing the boiling heat transfer and thermal conduction within the porous layer. Zhai [120] also presented a correlation that considers the effects of vapor flow and porous layer structure.

Kovalyov and Soloviyov [121] proposed a more rationally based model. They proposed that the pores in the matrix could be filled either liquid or vapor, depending on whether the pore is larger than the critical meniscus size; then, the vapor formed at the menisci within the matrix flows to the surface forced by "capillary pressure" and forms bubbles at the surface. The model can provide predictions for the heat transfer performance of a porous surface having a varied thermal conductivity, permeability, and thickness. Webb [7] regarded this work as an important contribution in understanding of the boiling mechanism in porous structures.

Polyaev and Kichatov [122] developed a semi-empirical model for boiling on surfaces with porous coatings. The model assumes that the total thermal load supplied is spent only in vaporization, and that the vaporization only takes place in the porous coating. The model uses Darcy's law, which describes flow of a fluid through a porous medium, to relate the pressure drop to the velocity of the escaping vapor. The model also formulates the critical conditions for the boiling regime transitions.

Rainey et al. [123] proposed a correlation to fit their pool boiling data of FC-72 on a microporous-coated surface. The correlation simply relates the heat flux with superheat and pressure, and it does not account for the fluid properties or the coating structure parameters.

Zhang et al. [124] proposed a mechanistic model for the boiling heat transfer on a sponge-like nanoporous coated surface. Based on the model of Nakayama et al. [97], this model includes a new term

to account for the thin liquid film evaporation inside the pores. The new term incorporates the contact angle that reflects the wettability of the surface, which is not included in the model of Nakayama et al. [97].

5. Conclusions and suggestions

Commercial use of enhanced boiling surfaces has driven improvements in surface development, boiling measurements, and predictive methods to make it the leading technology for augmenting boiling heat transfer. Researchers have introduced and studied a variety of enhanced surfaces, which can be classified by two basic types: structured surfaces and porous surfaces. Several commercially-available tubes for enhanced pool boiling have been extensively used in the refrigeration industry, like the GEWA series, Turbo-B series, Thermoexcel-E, and High-Flux. Many novel techniques capable of producing micro/nano-scale structures have been reported but still require further investigation to make commercial manufacture possible. With the trend of the enhanced geometries being more and more complex, the development of accurate predictive models becomes more challenging. The fundamentals in the related areas such as fouling and oil effect on enhanced surfaces need to be further developed.

Presently, low-GWP refrigerant enhanced pool boiling studies exist primarily for HC refrigerants. The number of studies with HFO is smaller than those for HC refrigerants, but has been increasing since 2010. Few studies on NH₃ and CO₂ were found in the open literature. From a general overview, enhanced surfaces produce a significant enhancement in the pool boiling heat transfer of low-GWP refrigerants. The reported enhancement factors vary from 1 to 10, depending on the enhanced geometry and the refrigerant. Nevertheless, the current database still needs to be expanded to cover more refrigerants, surfaces, and conditions.

Many mechanistic based models have been established for structured surfaces while relatively fewer have been developed for porous surfaces. These models are useful for understanding the enhanced boiling mechanisms, predicting the heat transfer performance, and for designing high-performance geometries. There are also some correlations for both structured and porous surfaces but most of them are not based on a database consisting of low-GWP refrigerants. The prediction accuracy of these correlations for low-GWP refrigerants needs to be examined in future studies.

Conflict of interest

None.

Acknowledgement

This work was funded by the National Institute of Standards and Technology (NIST), United States. Thanks go to D. Han of Ingersoll Rand and to the following NIST personnel for their constructive criticism of the draft manuscript: W. Healy and P. Domanski.

References

- [1] European Parliament, Regulation (EU) No. 517/2014 of the European Parliament and of the Council of 16 April 2014 on fluorinated greenhouse gases and repealing Regulation (EC) No. 842/2006, Off. J. Eur. Union. L150 (2014) 195–230.
- [2] United Nations Environment Programme (UNEP), Further Amendment of the Montreal Protocol, in: Twenty-Eighth Meet. Parties to Montr. Protoc. Subst. That Deplete Ozone Layer, Kigali, 2016: p. UNEP/OzL.Pro.28/CRP/10. <<http://conf.montreal-protocol.org/meeting/mop/mop-28/crps/SitePages/Home.aspx>>.
- [3] U.S. Environmental Protection Agency (EPA), Protection of Stratospheric Ozone: Revision to References for Refrigeration and Air Conditioning Sector To Incorporate Latest Edition of Certain Industry, Consensus-Based Standards, Fed. Regist. 83 (2018) 38969–38976.
- [4] A. Mota-Babiloni, J. Navarro-Esbrí, F. Molés, Á.B. Cervera, B. Peris, G. Verdú, A review of refrigerant R1234ze(E) recent investigations, Appl. Therm. Eng. 95 (2016) 211–222, <https://doi.org/10.1016/j.applthermaleng.2015.09.055>.
- [5] Z. Ayub, Current and future prospects of enhanced heat transfer in ammonia systems, Int. J. Refrig. 31 (2008) 652–657, <https://doi.org/10.1016/j.ijrefrig.2007.11.012>.
- [6] A. Mota-Babiloni, P. Makhnatch, R. Khodabandeh, Recent investigations in HFCs substitution with lower GWP synthetic alternatives: focus on energetic performance and environmental impact, Int. J. Refrig. 82 (2017) 288–301, <https://doi.org/10.1016/j.ijrefrig.2017.06.026>.
- [7] R.L. Webb, N.-H. Kim, *Principles of Enhanced Heat Transfer*, second ed., Taylor & Francis, New York, 2005.
- [8] R.L. Webb, Donald Q. Kern, Lecture award paper: odyssey of the enhanced boiling surface, J. Heat Transf. 126 (2004) 1051, <https://doi.org/10.1115/1.1834615>.
- [9] M. Shojaeian, A. Koşar, Pool boiling and flow boiling on micro- and nanostructured surfaces, Exp. Therm. Fluid Sci. 63 (2015) 45–73, <https://doi.org/10.1016/j.expthermflusci.2014.12.016>.
- [10] K.C. Leong, J.Y. Ho, K.K. Wong, A critical review of pool and flow boiling heat transfer of dielectric fluids on enhanced surfaces, Appl. Therm. Eng. 112 (2017) 999–1019, <https://doi.org/10.1016/j.applthermaleng.2016.10.138>.
- [11] R. Saidur, S.N. Kazi, M.S. Hossain, M.M. Rahman, H.A. Mohammed, A review on the performance of nanoparticles suspended with refrigerants and lubricating oils in refrigeration systems, Renew. Sustain. Energy Rev. 15 (2011) 310–323, <https://doi.org/10.1016/j.rser.2010.08.018>.
- [12] W.H. Azmi, M.Z. Sharif, T.M. Yusof, R. Mamat, A.A.M. Redhwan, Potential of nanorefrigerant and nanolubricant on energy saving in refrigeration system – a review, Renew. Sustain. Energy Rev. 69 (2017) 415–428, <https://doi.org/10.1016/j.rser.2016.11.207>.
- [13] Varun, M.O. Garg, H. Nautiyal, S. Khurana, M.K. Shukla, Heat transfer augmentation using twisted tape inserts: a review, Renew. Sustain. Energy Rev. 63 (2016) 193–225, <https://doi.org/10.1016/j.rser.2016.04.051>.
- [14] C.Y. Zhao, Review on thermal transport in high porosity cellular metal foams with open cells, Int. J. Heat Mass Transf. 55 (2012) 3618–3632, <https://doi.org/10.1016/j.ijheatmasstransfer.2012.03.017>.
- [15] S. Liu, M. Sakr, A comprehensive review on passive heat transfer enhancements in pipe exchangers, Renew. Sustain. Energy Rev. 19 (2013) 64–81, <https://doi.org/10.1016/j.rser.2012.11.021>.
- [16] M. Sheikholeslami, M. Gorji-Bandpy, D.D. Ganji, Review of heat transfer enhancement methods: focus on passive methods using swirl flow devices, Renew. Sustain. Energy Rev. 49 (2015) 444–469, <https://doi.org/10.1016/j.rser.2015.04.113>.
- [17] M. Legay, N. Gondrexon, S. Le Person, P. Boldo, A. Bontemps, Enhancement of heat transfer by ultrasound: review and recent advances, Int. J. Chem. Eng. 2011 (2011) 1–17, <https://doi.org/10.1155/2011/670108>.
- [18] C. Guo, X. Hu, W. Cao, D. Yu, D. Tang, Effect of mechanical vibration on flow and heat transfer characteristics in rectangular microgrooves, Appl. Therm. Eng. 52 (2013) 385–393, <https://doi.org/10.1016/j.applthermaleng.2012.12.010>.
- [19] W. Liu, Z. Yang, B. Zhang, P. Lv, Experimental study on the effects of mechanical vibration on the heat transfer characteristics of tubular laminar flow, Int. J. Heat Mass Transf. 115 (2017) 169–179, <https://doi.org/10.1016/j.ijheatmasstransfer.2017.07.025>.
- [20] S. Laohalerdtdecha, P. Naphon, S. Wongwises, A review of electrohydrodynamic enhancement of heat transfer, Renew. Sustain. Energy Rev. 11 (2007) 858–876, <https://doi.org/10.1016/j.rser.2005.07.002>.
- [21] L. Léal, M. Miscevic, P. Lavieille, M. Amokrane, F. Pigache, F. Topin, B. Nogarède, L. Tadrist, An overview of heat transfer enhancement methods and new perspectives: focus on active methods using electroactive materials, Int. J. Heat Mass Transf. 61 (2013) 505–524, <https://doi.org/10.1016/j.ijheatmasstransfer.2013.01.083>.
- [22] A.E. Kabeel, E.M.S. El-Said, S.A. Dafea, A review of magnetic field effects on flow and heat transfer in liquids: present status and future potential for studies and applications, Renew. Sustain. Energy Rev. 45 (2015) 830–837, <https://doi.org/10.1016/j.rser.2015.02.029>.
- [23] D. Gorenflo, S. Kottthoff, Review on pool boiling heat transfer of carbon dioxide, Int. J. Refrig. 28 (2005) 1169–1185, <https://doi.org/10.1016/j.ijrefrig.2005.09.008>.
- [24] M. Jakob, *Heat Transfer*, John Wiley & Sons, New York, 1949.
- [25] C. Carty, A.S. Foust, Surface variables in nucleate boiling, Chem. Eng. Prog. Symp. Ser. 51 (1955) 1–12.
- [26] H.M. Kurihara, J.E. Myers, The effects of superheat and surface roughness on boiling coefficients, AIChE J. 6 (1960) 83–91, <https://doi.org/10.1002/aic.690060117>.
- [27] P. Griffith, J.D. Wallis, The role of surface conditions in nucleate boiling, Chem. Eng. Prog. Symp. Ser. 56 (1960) 49–63.
- [28] J.E. Benjamin, *Bubble Growth in Nucleate Boiling of a Binary Mixture*, University of Illinois at Urbana-Champaign, USA, 1960.
- [29] P.J. Berenson, Experiments on pool-boiling heat transfer, Int. J. Heat Mass Transf. 5 (1962) 985–999, [https://doi.org/10.1016/0017-9310\(62\)90079-0](https://doi.org/10.1016/0017-9310(62)90079-0).
- [30] P.J. Marto, W.M. Rohsenow, Effects of surface conditions on nucleate pool boiling of sodium, J. Heat Transfer 88 (1966) 196, <https://doi.org/10.1115/1.3691514>.
- [31] R.M. Milton, Heat exchange system, U.S. Patent 3384154A, 1968.

- [32] R.L. Webb, The evolution of enhanced surface geometries for nucleate boiling, *Heat Transf. Eng.* 2 (1981) 46–69, <https://doi.org/10.1080/01457638108962760>.
- [33] R.L. Webb, Nucleate boiling on porous coated surfaces, *Heat Transf. Eng.* 4 (1983) 71–82, <https://doi.org/10.1080/01457638108939610>.
- [34] M.A. Kedzierski, L. Lin, D. Kang, Pool boiling of low-GWP replacements for R134a on a reentrant cavity surface; extensive measurement and analysis, NIST Tech. Note 1968 (2017), <https://doi.org/10.6028/NIST.TN.1968>.
- [35] S.I. Haider, A Theoretical and Experimental Study of Nucleate Pool Boiling Enhancement on Structured Surfaces, The Pennsylvania State University, 1994.
- [36] M.A. Kedzierski, Calorimetric and Visual Measurements of R123 Pool Boiling on Four Enhanced Surfaces, Washington D.C., USA, 1995.
- [37] M. Saier, H.-W. Kastner, R. Klockler, Y and T-finned tubes and methods and apparatus for their making, US4179911A, 1979.
- [38] Wieland-Werke Ag., GEWA-B Evaporator Tubes, 2017. <http://www.wieland-thermalsolutions.com/mediaPool/content/media/en/prospekte/hochleistungsrohre/High_Performance_Boiling_Tubes_GEWA_B.pdf>.
- [39] K. Fujie, W. Nakayama, H. Kuwahara, K. Kakizaki, Heat transfer wall for boiling liquids, U.S. Patent 4060125, 1977.
- [40] J.L. Cunningham, B.J. Campbell, Method of making heat transfer tube with improved outside surface for nucleate boiling, U.S. Patent 4729155, 1988.
- [41] P. Thors, N.R. Clevinger, B.J. Campbell, J.T. Tyler, Heat transfer tubes and methods of fabrication thereof, U.S. patent 5697430, 1997.
- [42] J.R. Thome, *Enhanced Boiling Heat Transfer*, Hemisphere, New York, 1990.
- [43] D.E. Kim, D.I. Yu, D.W. Jerng, M.H. Kim, H.S. Ahn, Review of boiling heat transfer enhancement on micro/nanostructured surfaces, *Exp. Therm. Fluid Sci.* 66 (2015) 173–196, <https://doi.org/10.1016/j.expthermfluidsci.2015.03.023>.
- [44] L.L. Vasiliiev, A.S. Zhuravlyov, M.N. Novikov, A.V. Ovsianik, L.L. Vasiliiev, An experimental investigation of the hydrocarbons pool boiling on porous structures, in: *Proceeding 12th Int. Heat Transf. Conf., Grenoble, France, 2002*, pp. 623–628.
- [45] R.M. Milton, Heat exchange system, U.S. Patent 3523577A, 1970.
- [46] R.M. Milton, Heat exchange system with porous boiling layer, U.S. Patent 3587730A, 1971.
- [47] C. Li, G.P. Peterson, Evaporation/boiling in thin capillary wicks (II)—effects of volumetric porosity and mesh size, *J. Heat Transfer* 128 (2006) 1320, <https://doi.org/10.1115/1.2349508>.
- [48] W.T. Ji, Z.G. Qu, Z.Y. Li, J.F. Guo, D.C. Zhang, W.Q. Tao, Pool boiling heat transfer of R134a on single horizontal tube surfaces sintered with open-celled copper foam, *Int. J. Therm. Sci.* 50 (2011) 2248–2255, <https://doi.org/10.1016/j.jthermalsci.2011.05.018>.
- [49] P. Vuoristo, Thermal spray coating processes, in: *Compr. Mater. Process., Elsevier*, 2014, pp. 229–276, <https://doi.org/10.1016/B978-0-08-096532-1.00407-6>.
- [50] A.K. Dewangan, A. Kumar, R. Kumar, Nucleate boiling of pure and quasi-azetropic refrigerants from copper coated surfaces, *Appl. Therm. Eng.* 94 (2016) 395–403, <https://doi.org/10.1016/j.applthermaleng.2015.10.138>.
- [51] S.-S. Hsieh, C.-G. Ke, Bubble dynamic parameters and pool boiling heat transfer on plasma coated tubes in saturated R-134a and R-600a, *J. Heat Transfer* 124 (2002) 704, <https://doi.org/10.1115/1.1481360>.
- [52] C.A.D. Rodriguez, G. Tremiliosi-Filho, Electrochemical deposition, in: *Encycl. Tribol.*, Springer US, Boston, MA, 2013, pp. 918–922, https://doi.org/10.1007/978-0-387-92897-5_700.
- [53] Z. Yao, Y.-W. Lu, S.G. Kandlikar, Direct growth of copper nanowires on a substrate for boiling applications, *Micro Nano Lett.* 6 (2011) 563, <https://doi.org/10.1049/mnl.2011.0136>.
- [54] M.S. El-Genk, A.F. Ali, Enhanced nucleate boiling on copper micro-porous surfaces, *Int. J. Multiph. Flow* 36 (2010) 780–792, <https://doi.org/10.1016/j.ijmultiphaseflow.2010.06.003>.
- [55] J.R. Creighton, P. Ho, Introduction to chemical vapour deposition, in: *Chem. Vap. Depos.*, 2010, pp. 1–28, https://doi.org/10.1007/978-1-84882-894-0_1.
- [56] A.A. Balandin, S. Ghosh, W. Bao, I. Calizo, D. Teweldebrhan, F. Miao, C.N. Lau, Superior thermal conductivity of single-layer graphene, *Nano Lett.* 8 (2008) 902–907, <https://doi.org/10.1021/nl0731872>.
- [57] S. Ujereh, T. Fisher, I. Mudawar, Effects of carbon nanotube arrays on nucleate pool boiling, *Int. J. Heat Mass Transf.* 50 (2007) 4023–4038, <https://doi.org/10.1016/j.ijheatmasstransfer.2007.01.030>.
- [58] J.A. Weibel, S.S. Kim, T.S. Fisher, S.V. Garimella, Carbon nanotube coatings for enhanced capillary-fed boiling from porous microstructures, *Nanoscale Microscale Thermophys. Eng.* 16 (2012) 1–17, <https://doi.org/10.1080/15567265.2011.646000>.
- [59] C.M. Patil, S.G. Kandlikar, Review of the manufacturing techniques for porous surfaces used in enhanced pool boiling, *Heat Transf. Eng.* 35 (2014) 887–902, <https://doi.org/10.1080/01457632.2014.862141>.
- [60] H.M. Ali, M.Z. Qasim, Free convection condensation of steam on horizontal wire wrapped tubes: effect of wire thermal conductivity, pitch and diameter, *Appl. Therm. Eng.* 90 (2015) 207–214, <https://doi.org/10.1016/j.applthermaleng.2015.07.006>.
- [61] H.M. Ali, M.Z. Qasim, M. Ali, Free convection condensation heat transfer of steam on horizontal square wire wrapped tubes, *Int. J. Heat Mass Transf.* 98 (2016) 350–358, <https://doi.org/10.1016/j.ijheatmasstransfer.2016.03.053>.
- [62] M. Shafae, H. Mashouf, A. Sarmadian, S.G. Mohseni, Evaporation heat transfer and pressure drop characteristics of R-600a in horizontal smooth and helically dimpled tubes, *Appl. Therm. Eng.* 107 (2016) 28–36, <https://doi.org/10.1016/j.applthermaleng.2016.06.148>.
- [63] J. Darabi, M.M. Ohadi, M.A. Fanni, S.V. Dessiatoun, M.A. Kedzierski, Effect of heating boundary conditions on pool boiling experiments, *HVAC&R Res.* 5 (1999) 283–296, <https://doi.org/10.1080/10789669.1999.10391239>.
- [64] K.J. Park, D. Jung, Nucleate boiling heat transfer coefficients of R1234yf on plain and low fin surfaces, *Int. J. Refrig.* 33 (2010) 553–557, <https://doi.org/10.1016/j.ijrefrig.2009.12.020>.
- [65] D. Jung, H. Lee, D. Bae, S. Oho, Nucleate boiling heat transfer coefficients of flammable refrigerants, *Int. J. Refrig.* 27 (2004) 409–414, <https://doi.org/10.1016/j.ijrefrig.2003.11.007>.
- [66] D. Gorenflo, U. Chandra, S. Kotthoff, A. Luke, Influence of thermophysical properties on pool boiling heat transfer of refrigerants, *Int. J. Refrig.* 27 (2004) 492–502, <https://doi.org/10.1016/j.ijrefrig.2004.03.004>.
- [67] E. van Rooyen, J.R. Thome, Pool boiling data and prediction method for enhanced boiling tubes with R-134a, R-236fa and R-1234ze(E), *Int. J. Refrig.* 36 (2013) 447–455, <https://doi.org/10.1016/j.ijrefrig.2012.11.023>.
- [68] Y. Lee, D.-G. Kang, J.-H. Kim, D. Jung, Nucleate boiling heat transfer coefficients of HFO1234yf on various enhanced surfaces, *Int. J. Refrig.* 38 (2014) 198–205, <https://doi.org/10.1016/j.ijrefrig.2013.09.014>.
- [69] E. Goryg, Nucleate boiling of low GWP refrigerants on highly enhanced tube surface, *Int. J. Heat Mass Transf.* 96 (2016) 660–666, <https://doi.org/10.1016/j.ijheatmasstransfer.2016.01.057>.
- [70] R. Nagata, C. Kondou, S. Koyama, Enhancement of R1234ze(Z) pool boiling heat transfer on horizontal titanium tubes for high-temperature heat pumps, *Sci. Technol. Built Environ.* 23 (2017) 923–932, <https://doi.org/10.1080/23744731.2017.1325706>.
- [71] H.-W. Byun, D.H. Kim, S.H. Yoon, C.H. Song, K.H. Lee, O.J. Kim, Pool boiling performance of enhanced tubes on low GWP refrigerants, *Appl. Therm. Eng.* 123 (2017) 791–798, <https://doi.org/10.1016/j.applthermaleng.2017.05.009>.
- [72] M.A. Kedzierski, L. Lin, D. Kang, Pool boiling of low-global warming potential replacements for R134a on a reentrant cavity surface, *J. Heat Transfer* 140 (2018), <https://doi.org/10.1115/1.4040783> 121502.
- [73] M.A. Kedzierski, L. Lin, Pool boiling of HFO-1336mzz(Z) on a reentrant cavity surface; extensive measurement and analysis, Gaithersburg, MD, 2018. <https://doi.org/10.6028/NIST.TN.2022>.
- [74] G. Moreno, S. Narumanchi, C. King, Pool boiling heat transfer characteristics of HFO-1234yf on plain and microporous-enhanced surfaces, *J. Heat Transfer* 135 (2013), <https://doi.org/10.1115/1.4024622> 111014.
- [75] C. Kondou, S. Umamoto, S. Koyama, Y. Mitooka, Improving the heat dissipation performance of a looped thermosiphon using low-GWP volatile fluids R1234ze(Z) and R1234ze(E) with a super-hydrophilic boiling surface, *Appl. Therm. Eng.* 118 (2017) 147–158, <https://doi.org/10.1016/j.applthermaleng.2017.02.073>.
- [76] P. Hübner, W. Künstler, Pool boiling heat transfer at finned tubes: influence of surface roughness and shape of the fins, *Int. J. Refrig.* 20 (1997) 575–582, [https://doi.org/10.1016/S0140-7007\(97\)00033-9](https://doi.org/10.1016/S0140-7007(97)00033-9).
- [77] R. Mertz, R. Kulenovic, M. Groll, Enhanced boiling tubes with subsurface structures: investigation, visualization and industrial application, in: *Exp. Heat Transf. Fluid Mech. Thermodyn. 2001 Proc. 5th World Conf. Exp. Heat Transf. Fluid Mech., Thessaloniki, Greece, 2001*, pp. 871–876.
- [78] R. Mertz, R. Kulenovic, Y. Chen, M. Groll, Pool boiling of butane from enhanced evaporator tubes, in: *Heat Transf. 2002 Proc. 12th Int. Heat Transf. Conf., Grenoble, France, August 18–23, 2002*, pp. 629–634.
- [79] R. Kulenovic, R. Mertz, M. Groll, High speed flow visualization of pool boiling from structured tubular heat transfer surfaces, *Exp. Therm. Fluid Sci.* 25 (2002) 547–555, [https://doi.org/10.1016/S0894-1777\(01\)00113-3](https://doi.org/10.1016/S0894-1777(01)00113-3).
- [80] Y. Chen, M. Groll, R. Mertz, R. Kulenovic, Bubble dynamics of boiling of propane and iso-butane on smooth and enhanced tubes, *Exp. Therm. Fluid Sci.* 28 (2004) 171–178, [https://doi.org/10.1016/S0894-1777\(03\)00036-0](https://doi.org/10.1016/S0894-1777(03)00036-0).
- [81] Y. Chen, M. Groll, R. Mertz, R. Kulenovic, Pool boiling heat transfer of propane, isobutane and their mixtures on enhanced tubes with reentrant channels, *Int. J. Heat Mass Transf.* 48 (2005) 2310–2322, <https://doi.org/10.1016/j.ijheatmasstransfer.2004.10.037>.
- [82] Y. Chen, M. Groll, R. Mertz, R. Kulenovic, Visualization and mechanisms of pool boiling of propane, isobutane and their mixtures on enhanced tubes with reentrant channels, *Int. J. Heat Mass Transf.* 48 (2005) 2516–2528, <https://doi.org/10.1016/j.ijheatmasstransfer.2004.10.039>.
- [83] D. Jung, H. Lee, D. Bae, J. Ha, Nucleate boiling heat transfer coefficients of flammable refrigerants on various enhanced tubes, *Int. J. Refrig.* 28 (2005) 451–455, <https://doi.org/10.1016/j.ijrefrig.2004.07.024>.
- [84] S. Kotthoff, D. Gorenflo, E. Danger, A. Luke, Heat transfer and bubble formation in pool boiling: effect of basic surface modifications for heat transfer enhancement, *Int. J. Therm. Sci.* 45 (2006) 217–236, <https://doi.org/10.1016/j.ijthermalsci.2005.01.011>.
- [85] A. Luke, B.C.F. Müller, Heat transfer mechanisms of propane boiling on horizontal steel tubes with smooth and enhanced surfaces, in: *14th Int. Heat Transf. Conf., ASME*, 2010, pp. 553–561, <https://doi.org/10.1115/IHTC14-22887>.
- [86] X. Zhou, K. Bier, Pool boiling heat transfer from a horizontal tube coated with oxide ceramics, *Int. J. Refrig.* 20 (1997) 552–560, [https://doi.org/10.1016/S0140-7007\(97\)00023-6](https://doi.org/10.1016/S0140-7007(97)00023-6).
- [87] L.L. Vasiliiev, V.V. Khrolenok, A.S. Zhuravlyov, Intensification of heat transfer at propane pool boiling on single horizontal tubes, *Rev. Générale Therm.* 37 (1998) 962–967, [https://doi.org/10.1016/S0035-3159\(98\)80020-2](https://doi.org/10.1016/S0035-3159(98)80020-2).

- [88] S.-S. Hsieh, T.-Y. Yang, Nucleate pool boiling from coated and spirally wrapped tubes in saturated R-134a and R-600a at low and moderate heat flux, *J. Heat Transfer* 123 (2001) 257, <https://doi.org/10.1115/1.1351818>.
- [89] A.K. Dewangan, A. Kumar, R. Kumar, Experimental study of nucleate boiling heat transfer of R-134a and R-600a on thermal spray coating surfaces, *Int. J. Therm. Sci.* 110 (2016) 304–313, <https://doi.org/10.1016/j.ijthermalsci.2016.07.015>.
- [90] A.K. Dewangan, A. Kumar, R. Kumar, Pool boiling of iso-butane and quasi azeotropic refrigerant mixture on coated surfaces, *Exp. Therm. Fluid Sci.* 85 (2017) 176–188, <https://doi.org/10.1016/j.expthermflusci.2017.02.028>.
- [91] V.A. Djundin, A.G. Solov'ev, A.V. Borissanskaja, J. Vol'nykh, Influence of the type of surface on heat transfer in boiling, *Kholod Tekh.* 5 (1984) 33–37.
- [92] K. Spindler, Overview and discussion on pool boiling heat transfer data and correlations of ammonia, *Int. J. Refrig.* 33 (2010) 1292–1306, <https://doi.org/10.1016/j.ijrefrig.2010.06.012>.
- [93] G.N. Danilova, V.A. Dyundin, A.V. Borishanskaya, A.G. Soloviyov, Y.A. Vol'nykh, A.A. Kozyrev, Effect of surface conditions on boiling heat transfer of refrigerants in shell-and-tube evaporators, *Heat Transf. - Sov. Res.* 22 (1990) 56–65.
- [94] J. Zheng, M.-C. Chyu, Z. Ayub, Boiling of ammonia/lubricant mixture on a horizontal enhanced tube in a flooded evaporator with inlet vapor quality, *Int. J. Refrig.* 31 (2008) 564–572, <https://doi.org/10.1016/j.ijrefrig.2007.06.016>.
- [95] J. Fernández-Seara, Á.Á. Pardiñas, R. Diz, Heat transfer enhancement of ammonia pool boiling with an integral-fin tube, *Int. J. Refrig.* 69 (2016) 175–185, <https://doi.org/10.1016/j.ijrefrig.2016.05.012>.
- [96] S. Liu, Z. Dong, W. Zhang, Experimental research on CO₂ pool boiling heat transfer outside a single tube, in: *Micro/Nanofluidics Lab-on-a-Chip; Nanofluids; Micro/Nanoscale Interfacial Transp. Phenomena; Micro/Nanoscale Boil. Condens. Heat Transf. Micro/Nanoscale Therm. Radiation; Micro/Nanoscale Energy Devices Syst.*, vol. 1, ASME, 2016, p. V001T04A009, <https://doi.org/10.1115/MNHMT2016-6661>.
- [97] W. Nakayama, T. Daikoku, H. Kuwahara, T. Nakajima, Dynamic model of enhanced boiling heat transfer on porous surfaces – part II: analytical modeling, *J. Heat Transfer* 102 (1980) 451, <https://doi.org/10.1115/1.3244321>.
- [98] W. Nakayama, T. Daikoku, H. Kuwahara, T. Nakajima, Dynamic model of enhanced boiling heat transfer on porous surfaces—part I: experimental investigation, *J. Heat Transfer* 102 (1980) 445, <https://doi.org/10.1115/1.3244320>.
- [99] W. Nakayama, T. Daikoku, T. Nakajima, Effects of Pore Diameters and System Pressure on Saturated Pool Nucleate Boiling Heat Transfer From Porous Surfaces, *J. Heat Transfer* 104 (1982) 286, <https://doi.org/10.1115/1.3245085>.
- [100] M.-D. Xin, Y.-D. Chao, Analysis and experiment of boiling heat transfer on t-shaped finned surfaces, *Chem. Eng. Commun.* 50 (1987) 185–199, <https://doi.org/10.1080/00986448708911825>.
- [101] L.-H. Chien, R.L. Webb, A nucleate boiling model for structured enhanced surfaces, *Int. J. Heat Mass Transf.* 41 (1998) 2183–2195, [https://doi.org/10.1016/S0017-9310\(97\)00302-5](https://doi.org/10.1016/S0017-9310(97)00302-5).
- [102] C. Ramaswamy, Y. Joshi, W. Nakayama, W.B. Johnson, Semi-analytical model for boiling from enhanced structures, *Int. J. Heat Mass Transf.* 46 (2003) 4257–4269, [https://doi.org/10.1016/S0017-9310\(03\)00216-3](https://doi.org/10.1016/S0017-9310(03)00216-3).
- [103] S. Murthy, Y. Joshi, S. Gurrum, W. Nakayama, Enhanced boiling heat transfer simulation from structured surfaces: semi-analytical model, *Int. J. Heat Mass Transf.* 49 (2006) 1885–1895, <https://doi.org/10.1016/j.ijheatmasstransfer.2005.10.035>.
- [104] A.K. Das, P.K. Das, S. Bhattacharyya, P. Saha, Nucleate boiling heat transfer from a structured surface – effect of liquid intake, *Int. J. Heat Mass Transf.* 50 (2007) 1577–1591, <https://doi.org/10.1016/j.ijheatmasstransfer.2006.08.030>.
- [105] R. Pastuszko, M.E. Poniewski, Semi-analytical approach to boiling heat fluxes calculation in subsurface horizontal and vertical tunnels, *Int. J. Therm. Sci.* 47 (2008) 1169–1183, <https://doi.org/10.1016/j.ijthermalsci.2007.10.003>.
- [106] R. Pastuszko, Pool boiling for extended surfaces with narrow tunnels – visualization and a simplified model, *Exp. Therm. Fluid Sci.* 38 (2012) 149–164, <https://doi.org/10.1016/j.expthermflusci.2011.12.004>.
- [107] B.B. Milkic, W.M. Rohsenow, A new correlation of pool-boiling data including the effect of heating surface characteristics, *J. Heat Transfer* 91 (1969) 245, <https://doi.org/10.1115/1.3580136>.
- [108] R. Pastuszko, T.M. Wójcik, Experimental investigations and a simplified model for pool boiling on micro-fins with sintered perforated foil, *Exp. Therm. Fluid Sci.* 63 (2015) 34–44, <https://doi.org/10.1016/j.expthermflusci.2015.01.002>.
- [109] W. Fritz, Berechnung des Maximalvolumens von Dampfblasen, *Phys. Zeitschrift.* 36 (1935) 379–388.
- [110] K.N. Rainey, S.M. You, S. Lee, Effect of pressure, subcooling, and dissolved gas on pool boiling heat transfer from microporous, square pin-finned surfaces in FC-72, *Int. J. Heat Mass Transf.* 46 (2003) 23–35, [https://doi.org/10.1016/S0017-9310\(02\)00257-0](https://doi.org/10.1016/S0017-9310(02)00257-0).
- [111] M.Y. Wen, C.Y. Ho, Pool boiling heat transfer of deionized and degassed water in vertical/horizontal V-shaped geometries, *Heat Mass Transf. Und Stoffuebertragung.* 39 (2003) 729–736, <https://doi.org/10.1007/s00231-002-0358-z>.
- [112] K.G. Rajulu, R. Kumar, B. Mohanty, H.K. Varma, Enhancement of nucleate pool boiling heat transfer coefficient by reentrant cavity surfaces, *Heat Mass Transf.* 41 (2004) 127–132, <https://doi.org/10.1007/s00231-004-0526-4>.
- [113] M. Christians, J.R. Thome, Falling film evaporation on enhanced tubes, part 2: prediction methods and visualization, *Int. J. Refrig.* 35 (2012) 313–324, <https://doi.org/10.1016/j.ijrefrig.2011.10.019>.
- [114] J.Y. Ho, K.K. Wong, K.C. Leong, Saturated pool boiling of FC-72 from enhanced surfaces produced by Selective Laser Melting, *Int. J. Heat Mass Transf.* 99 (2016) 107–121, <https://doi.org/10.1016/j.ijheatmasstransfer.2016.03.073>.
- [115] P.S. O'Neill, C.F. Gottzmann, J.W. Terbot, Novel heat exchanger increases cascade cycle efficiency for natural gas liquefaction, in: *Adv. Cryog. Eng.*, Springer US, Boston, MA, 1972, pp. 420–437, https://doi.org/10.1007/978-1-4684-7826-6_44.
- [116] K. Cornwell, B.G. Nair, T.D. Patten, Observation of boiling in porous media, *Int. J. Heat Mass Transf.* 19 (1976) 236–238, [https://doi.org/10.1016/0017-9310\(76\)90121-6](https://doi.org/10.1016/0017-9310(76)90121-6).
- [117] T. Ito, K. Nishikawa, Enhanced heat transfer by nucleate boiling on a sintered metal layer, *Refrigeration* 612 (1978) 15–20 (in Japanese).
- [118] K. Nishikawa, T. Ito, Augmentation of nucleate boiling heat transfer by prepared surfaces, in: T. Mizushima, W.J. Yang (Eds.), *Heat Transf. III Energy Probl.*, Washington D.C., USA, 1982, pp. 111–118.
- [119] G. Zhai, *Investigation of Enhanced Nucleate Boiling Heat Transfer on Porous Surface*, Tianjin University, 1982.
- [120] G. Zhai, R. Lin, Y. Cai, Investigation of nucleate boiling heat transfer on sintered porous surfaces, *J. Tianjin Univ.* 3 (1987) 63–70.
- [121] S.A. Kovalyov, S.L. Soloviyov, Heat transfer and critical heat fluxes in boiling on a porous surface, *Heat Transf. - Sov. Res.* 22 (1990) 364–375.
- [122] V.M. Polyakov, B.V. Kichatov, Boiling of a liquid on surfaces with porous coatings, *J. Eng. Phys. Thermophys.* 73 (2000) 253–258, <https://doi.org/10.1007/BF02681726>.
- [123] K.N. Rainey, S.M. You, S. Lee, Effect of pressure, subcooling, and dissolved gas on pool boiling heat transfer from microporous surfaces in FC-72, *J. Heat Transfer* 125 (2003) 75, <https://doi.org/10.1115/1.1527890>.
- [124] B.J. Zhang, K.J. Kim, H. Yoon, Enhanced heat transfer performance of alumina sponge-like nano-porous structures through surface wettability control in nucleate pool boiling, *Int. J. Heat Mass Transf.* 55 (2012) 7487–7498, <https://doi.org/10.1016/j.ijheatmasstransfer.2012.07.053>.
- [125] S.H. Kim, G.C. Lee, J.Y. Kang, H.S. Park, M.H. Kim, A study of nucleate bubble growth on microstructured surface through high speed and infrared visualization, *Int. J. Multiph. Flow* 95 (2017) 12–21, <https://doi.org/10.1016/j.ijmultiphaseflow.2017.02.007>.
- [126] C.M. Kruse, T. Anderson, C. Wilson, C. Zuhlke, D. Alexander, G. Gogos, S. Ndao, Enhanced pool-boiling heat transfer and critical heat flux on femtosecond laser processed stainless steel surfaces, *Int. J. Heat Mass Transf.* 82 (2015) 109–116, <https://doi.org/10.1016/j.ijheatmasstransfer.2014.11.023>.
- [127] C.K. Yu, D.C. Lu, T.C. Cheng, Pool boiling heat transfer on artificial micro-cavity surfaces in dielectric fluid FC-72, *J. Micromech. Microeng.* 16 (2006) 2092–2099, <https://doi.org/10.1088/0960-1317/16/10/024>.
- [128] Intergovernmental Panel on Climate Change (IPCC), ed., *Climate Change 2007 – The Physical Science Basis*, Cambridge University Press, Cambridge, 2007.
- [129] Intergovernmental Panel on Climate Change (IPCC), ed., *Climate Change 2013 – The Physical Science Basis*, Cambridge University Press, Cambridge, 2014, <https://doi.org/10.1017/CBO9781107415324>.